

Algorithmic methods to infer the evolutionary trajectories in cancer progression

Giulio Caravagna^{1,2,*} Alex Graudenzi^{1,3} Daniele Ramazzotti¹
 Rebeca Sanz-Pamplona⁴ Luca De Sano¹ Giancarlo Mauri^{1,5}
 Victor Moreno^{4,6} Marco Antoniotti^{1,7} Bud Mishra⁸

November 17, 2018

¹ Department of Informatics, Systems and Communication, University of Milan-Bicocca, Milan, Italy.

² School of Informatics, University of Edinburgh, Edinburgh, UK.

³ Institute of Molecular Bioimaging and Physiology of the Italian National Research Council (IBFM-CNR), Milan, Italy.

⁴ Unit of Biomarkers and Susceptibility, Cancer Prevention and Control Program, Catalan Institute of Oncology (ICO), IDIBELL & CIBERESP. Hospitalet de Llobregat, Barcelona, Spain.

⁵ SYSBIO Centre of Systems Biology, Milano, Italy.

⁶ Department of Clinical Sciences, Faculty of Medicine, University of Barcelona, Barcelona, Spain.

⁷ Milan Center for Neuroscience, University of Milan-Bicocca, Milan, Italy.

⁸ Courant Institute of Mathematical Sciences, New York University, New York, USA.

* Corresponding author, giulio.caravagna@ed.ac.uk.

Contents

1	Introduction	3
2	The PicNic pipeline	6
2.1	Reducing inter-tumor heterogeneity by cohort subtyping	6
2.2	Selection of driver events	7
2.3	Fitness equivalence of exclusive alterations	7
2.4	Progression inference and confidence estimation	9
3	Results	10
3.1	Evolution in a population of MSI/MSS colorectal tumors.	10
4	Discussion	12
5	Materials and methods	14
A	Reproducing this study	28
B	Glossary	29
C	PicNic's implementation for COADREAD samples	31
C.1	TCGA COADREAD project data	31
C.2	Driver events selection	32
C.3	Mutual exclusivity groups of alterations.	32

C.4	CAPRI's execution	33
D	Statistical validation of the models	34
D.1	Edge p-values	34
D.2	Bootstrap	35
D.3	Cross-validation	36
E	Supplementary Tables and Figures	37

List of Figures

1	Problem statement and overview of the PicNic pipeline	22
2	The PicNic pipeline	23
3	Data processed for MSI-HIGH tumors	24
4	Progression of MSS tumors	25
5	Progression of MSI-HIGH tumors	26
S6	PicNic pipeline processing MSI-HIGH/MSS tumors	40
S7	Mutations annotated by TCGA for the driver genes	41
S8	Lolliplot diagrams of TCGA mutations	42
S9	Groups of exclusive alterations for MSS tumors	43
S10	Selected data for MSS tumors	44
S11	Non-parametric bootstrap scores for MSS progression	45
S12	Non-parametric bootstrap scores for MSI-HIGH progression	46
S13	COADREAD statistics for models confidence	47
S14	Entropy loss for MSI-HIGH/MSS models	48
S15	Prediction error for each parent set of BIC and AIC models of MSS tumors	49
S16	Prediction error for each parent set of BIC and AIC models of MSI tumors	50
S17	Models and the phenotype that they might explain	51

Abstract

The genomic evolution inherent to cancer relates directly to a renewed focus on the voluminous next generation sequencing (NGS) data, and machine learning for the inference of explanatory models of how the (epi)genomic events are choreographed in cancer initiation and development. However, despite the increasing availability of multiple additional -omics data, this quest has been frustrated by various theoretical and technical hurdles, mostly stemming from the dramatic heterogeneity of the disease. In this paper, we build on our recent works on “selective advantage” relation among driver mutations in cancer progression and investigate its applicability to the modeling problem at the population level. Here, we introduce PiCnIc (Pipeline for Cancer Inference), a versatile, modular and customizable pipeline to extract ensemble-level progression models from cross-sectional sequenced cancer genomes. The pipeline has many translational implications as it combines state-of-the-art techniques for sample stratification, driver selection, identification of fitness-equivalent exclusive alterations and progression model inference. We demonstrate PiCnIc’s ability to reproduce much of the current knowledge on colorectal cancer progression, as well as to suggest novel experimentally verifiable hypotheses.

KEYWORDS: Cancer evolution; Selective advantage; Bayesian Structural Inference

STATEMENT OF SIGNIFICANCE: *A causality based new machine learning Pipeline for Cancer Inference (PicNic) is introduced to infer the underlying somatic evolution of ensembles of tumors from next generation sequencing data. PicNic combines techniques for sample stratification, driver selection and identification of fitness-equivalent exclusive alterations to exploit a novel algorithm based on Suppes’ probabilistic causation. The accuracy and translational significance of the results are studied in details, with an application to colorectal cancer. PicNic pipeline has been made publicly accessible for reproducibility, interoperability and for future enhancements.*

1 Introduction

Since the late seventies evolutionary dynamics, with its interplay between variation and selection, has progressively provided the widely-accepted paradigm for the interpretation of cancer emergence and development [1–3]. Random alterations of an organism’s (epi)genome can sometimes confer a functional *selective advantage*¹ to certain cells, in terms of adaptability and ability to survive and proliferate. Since the consequent *clonal expansions* are naturally constrained by the availability of resources (metabolites, oxygen, etc.), further mutations in the emerging heterogeneous tumor populations are necessary to provide additional *fitness* of different kinds that allow survival and proliferation in the unstable micro environment. Such further advantageous mutations will eventually allow some of their sub-clones to outgrow the competing cells, thus enhancing tumor’s heterogeneity as well as its ability to overcome future limitations imposed by the rapidly exhausting resources. Competition, predation, parasitism and cooperation have been in fact theorized as co-present among cancer clones [4].

In the well-known vision of Hanahan and Weinberg [5,6], the phenotypic stages that characterize this multistep evolutionary process are called *hallmarks*. These can be acquired by cancer cells in many possible alternative ways, as a result of a complex biological interplay at several spatio-temporal scales that is still only partially deciphered [7]. In this framework, we distinguish

¹For this and other technical terms commonly used in the statistics and cancer biology communities we provide a Glossary in the Supplementary Material.

“alterations” driving the hallmark acquisition process (i.e., *drivers*) by activating *oncogenes* or inactivating *tumor suppressor genes*, from those that are transferred to sub-clones without increasing their fitness (i.e., *passengers*) [8]. Driver identification is a modern challenge of cancer biology, as distinct cancer types exhibit very different combinations of drivers, some cancers display mutations in hundreds of genes [9], and the majority of drivers is mutated at low frequencies (“long tail” distribution), hindering their detection only from the statistics of the recurrence at the population-level [10].

Cancer clones harbour distinct types of alterations. The *somatic* (or *genetic*) ones involve either few nucleotides or larger chromosomal regions. They are usually catalogued as *mutations* - i.e., single nucleotide or structural variants at multiple scales (insertions, deletions, inversions, translocations) - of which only some are detectable as *Copy Number Alterations* (CNAs), most prevalent in many tumor types [11]. Also *epigenetic* alterations, such as *DNA methylation* and *chromatin reorganization*, play a key role in the process [12]. The overall picture is confounded by factors such as *genetic instability* [13], *tumor-microenvironment* interplay [14,15], and by the influence of *spatial organization* and *tissue specificity* on tumor development [16]².

Significantly, in many cases, distinct driver alterations can damage in a similar way the same *functional pathway*, leading to the acquisition of new hallmarks [17–21]. Such alterations individually provide an equivalent *fitness gain* to cancer cells, as any additional alteration hitting the same pathway would provide no further selective advantage. This dynamic results in groups of driver alterations that form *mutually exclusive* patterns across tumor samples from different patients (i.e., the sets of alterations that are involved in the same pathways tend not to occur mutated together). This phenomenon has significant translational consequences.

An immediate challenge posed by this state of affairs is the dramatic *heterogeneity* of cancer, both at the *inter-tumor* and at the *intra-tumor* levels [22]. The former manifests as different patients with the same cancer type can display few common alterations. This observation led to the development of techniques to stratify tumors into *subtypes* with different genomic signatures, prognoses and response to therapy [23]. The latter form of heterogeneity refers to the observed genotypic and phenotypic variability among the cancer cells within a single neoplastic lesion, characterized by the coexistence of more than one cancer clones with distinct evolutionary histories [24].

Cancer heterogeneity poses a serious problem from the diagnostic and therapeutic perspective as, for instance, it is now acknowledged that a single biopsy might not be representative of other parts of the tumor, hindering the problem of devising effective treatment strategies [4]. Therefore, presently the quest for an extensive etiology of cancer heterogeneity and for the identification of cancer evolutionary trajectories is central to cancer research, which attempts to exploit the massive amount of sequencing data available through public projects such as The Cancer Genome Atlas (TCGA) [25].

Such projects involve an increasing number of *cross-sectional* (epi)genomic profiles collected via single biopsies of patients with various cancer types, which might be used to extract trends of cancer evolution across a population of samples³. Higher resolution data such as *multiple samples* collected from the same tumor [24], as well as *single-cell* sequencing data [26], might be complementarily used to face the same problem within a specific patient. However, the lack of public data coupled

²We mention that much attention has been recently casted on newly discovered cancer genes affecting global processes that are apparently not directly related to cancer development, such as cell signaling, chromatin and epigenomic regulation, RNA splicing, protein homeostasis, metabolism and lineage maturation [10].

³At the time of this writing, in TCGA, sample sizes per cancer type are in the order of a few hundreds. Such numbers are expected to increase in the near future, with a clear benefit for all the statistical approaches to analyze cancer data which currently lack a proper background of data.

to the problems of accuracy and reliability, currently prevents a straightforward application [27].

These different perspectives lead to the different mathematical formulations of the problem of *inferring a cancer progression model* from genomic data, and a need for versatile computational tools to analyze data reproducibly – two intertwined issues examined at length in this paper [28]. Indeed, such models and tools can be focused either on characteristics of a population, i.e. *ensemble-level*, or on multiple clonality in a *single-patient*. In general, both problems deal with understanding the *temporal ordering of somatic alterations* accumulating during cancer evolution, but use orthogonal perspectives and different input data – see Figure 1 for a comparison. This paper proposes a new computational approach to efficiently deal with various aspects of the problem at a patient population level, relegating the other aspects to future publications.

Ensemble-level cancer evolution. It is thus desirable to extract a *probabilistic graphical model* explaining the statistical trend of accumulation of somatic alterations in a population of n cross-sectional samples collected from patients diagnosed with a specific cancer. To normalize against the experimental conditions in which tumors are sampled, we only consider the *list of alterations detected per sample* – thus, as 0/1 Bernoulli random variables.

Much of the difficulty lies in estimating the true and unknown trends of *selective advantage* among genomic alterations in the data, from such observations. This hurdle is not unsurmountable, if we constrain the scope to only those alterations that are *persistent across tumor evolution in all sub-clonal populations*, since it yields a consistent model of a temporal ordering of mutations. Therefore, epigenetic and transcriptomic states, such as hyper and hypo-methylations or over and under expression, could only be used, provided that they are persistent through tumor development [29].

Historically, the linear model of colorectal tumor progression by Vogelstein is an instance of an early solution to the cancer progression problem [30]. That approach was later generalized to accommodate *tree-models of branched evolution* [31–34] and later, further generalized to the inference of *directed acyclic graph* models, with several distinct strategies [35–38]. We contributed to this research program with the Cancer Progression Extraction with Single Edges (CAPRESE) and the Cancer Progression Inference (CAPRI) algorithms, which are currently implemented in TRONCO, an open source R package for Translational Oncology available in standard repositories [39–41]. Both techniques rely on Suppes’ theory of probabilistic causation to define estimators of selective advantage [42], are robust to the presence of noise in the data and perform well even with limited sample sizes. The former algorithm exploits shrinkage-like statistics to extract a tree model of progression, the latter combines bootstrap and maximum likelihood estimation with regularization to extract general directed acyclic graphs that capture branched, independent and confluent evolution. Both algorithms represent the current state-of-the-art approach to this problem, as they outperform others in speed, scale and predictive accuracy.

Clonal architecture in individual patients. A closely related problem addresses the detection of clonal signatures and their prevalence in individual tumors, a problem complicated by *intra-tumor* heterogeneity.

Even though this phylogenetic version of the progression inference problem naturally relies on data produced from *single-cell sequencing* assays [43, 44], the majority of approaches still make use of *bulk sequencing* data, usually from multiple biopsies of the same tumors [24, 45]. Indeed, several approaches try to extract the clonal signature of single tumors from *allelic imbalance proportions*,

a problem made difficult as sequenced samples usually contain a large number of cells belonging to a collection of sub-clones resulting from the complex evolutionary history of the tumor [46–55].

We keep the current work focused on the inference of progression models at the ensemble level, and plan to return to this variant to the problem in another publication.

2 The PicNic pipeline

We report on the design, development and evaluation of the Pipeline for Cancer Inference (PicNic) to extract ensemble-level cancer progression models from cross-sectional data (Figure 1). PicNic is versatile, modular and customizable; it exploits state-of-the-art data processing and machine learning tools to:

1. identify *tumor subtypes* and then in each subtype;
2. select (epi)genomic events *relevant* to the progression;
3. identify groups of events that are likely to be observed as *mutually exclusive*;
4. infer *progression models* from groups and related data, and annotate them with associated statistical confidence.

All these steps are necessary to minimize the confounding effects of inter-tumor heterogeneity, which are likely to lead to wrong results when data is not appropriately pre-processed⁴.

In each stage of PicNic different techniques can be employed, alternatively or jointly, according to specific research goals, input data, and cancer type. Prior knowledge can be easily accommodated into our pipeline, as well as the computational tools discussed in the next subsections and summarized in Figure 2. The rationale is similar in spirit to workflows implemented by consortia such as TCGA to analyze huge populations of cancer samples [56, 57]. One of the main novelties of our approach, is the exploitation of groups of exclusive alterations as a proxy to detect fitness-equivalent trajectories of cancer progression. This strategy is only feasible by the hypothesis-testing features of the recently developed CAPRI algorithm, an algorithm uniquely addressing this crucial aspect of the ensemble-level progression inference problem [40].

In the Results section, we study in details a specific use-case for the pipeline, processing colorectal cancer data from TCGA, where it is able to re-discover much of the existing body of knowledge about colorectal cancer progression. Based on the output of this pipeline, we also propose novel experimentally-verifiable hypotheses.

2.1 Reducing inter-tumor heterogeneity by cohort subtyping

In general, for each of n tumors (patients) we assume relevant (epi)genetic data to be available. We do not put constraints on data gathering and selection, leaving the user to decide the appropriate “resolution” of the input data. For instance, one might decide whether somatic mutations should be classified by type or by location, or aggregated. Or, one might decide to lift focal CNAs to

⁴The genuine selectivity relationship sought to be inferred are subject to the vagaries of Simpson’s paradox; it can change, or worst reverse, when we try to infer them from data not suitably pre-processed. This effect (due to such paradox) manifests as data are sampled from a highly heterogenous mixture of populations of cells [40]. PicNic uses various mechanisms to avoid these pitfalls. In this context, it should be pointed out that input bulk sequencing data suffers also from intra-tumor heterogeneity issues, which are unfortunately intrinsic to the technology.

the lower resolution of cytobands or full arms (e.g., in a kidney cancer cohort where very long CNAs are more common than focal events [58]). These choices depend on data and on the overall understanding of such alterations and their functional effects for the cancer under study, and no single all-encompassing rationale may be provided.

With these data at hand, we might wish to identify cancer subtypes in the *heterogeneous mixture* of input samples. In some cases the classification can benefit from clinical biomarkers, such as evidences of certain cell types [59], but in most cases we will have to rely on multiple *clustering* techniques at once, see, e.g., [56,57]. Many common approaches cluster expression profiles [60], often relying on non-negative matrix factorization techniques [61] or earlier approaches such as *k*-means, Gaussians mixtures or hierarchical/spectral clustering - see the review in [62]. For glioblastoma and breast cancer, for instance, mRNA expression subtypes provides good correlation with clinical phenotypes [63–65]. However, this is not always the case as, e.g., in colorectal cancer such clusters mismatch with survival and chemotherapy response [63]. Clustering of *full exome* mutation profiles or smaller panels of genes might be an alternative as it was shown for ovarian, uterine and lung cancers [66,67].

Using pipelines such as PicNic, we expect that the resulting subtypes will be routinely investigated, eventually leading to distinct progression models, which shall be characteristic of the population-level trends of cancer initiation and progression.

2.2 Selection of driver events

In subtypes detection, it becomes easier to find similarities across input samples when more alterations are available, as features selection gains precision. In progression inference, instead, one wishes to focus on $m \ll n$ *driver* alterations, which ensure also an appropriate statistical ratio between sample size (n , here the subtype size) and problem dimension (m).

Multiple tools filter out driver from passenger mutations. MutSigCV identifies drivers mutated more frequently than background mutation rate [68]. OncodriveFM avoids such estimation but looks for functional mutations [69]. OncodriveCLUST scans mutations clustering in small regions of the protein sequence [70]. MuSiC uses multiple types of clinical data to establish correlations among mutation sites, genes and pathways [71]. Some other tools search for driver CNAs that affect protein expression [72]. All these approaches use different statistical measures to estimate signs of positive selection, and we suggest using them in an orchestrated way, as done by platforms such as Intogen [73].

We anticipate that such tools will run independently on each subtype, as driver genes will likely differ across them, mimicking the different molecular properties of each group of samples; also, lists of genes produced by these tools might be augmented with prior knowledge about tumor suppressors or oncogenes.

2.3 Fitness equivalence of exclusive alterations

When working at the ensemble-level, identification of “groups of mutually exclusive” alterations is crucial to derive a correct inference. This step of PicNic is another attempt to resolve part of the inter-tumor heterogeneity, as such alterations *could* lead to the same phenotype (i.e., hence resulting “equivalent” in terms of progression), despite being genotypically “alternative”, i.e., exclusive, across the input cohort. This information shall be used to detect alternative routes to cancer progression which capture the specificities of individual patients.

A plethora of recent tools can be used to detect groups of fitness equivalent alterations, according to the data available for each subtype; greedy approaches [74, 75] or their optimizations, such as MEMO, which constrain search-space with network priors [76]. This strategy is further improved in MUTEX, which scans mutations and focal CNAs for genes with a common downstream effect in a curated signalling network, and selects only those genes that significantly contributes to the exclusivity pattern [77]. Other tools such as Dendrix, MDPFinder, Multi-Dendrix, CoMet, MEGSA or ME, employ advanced statistics or generative approaches without priors [78–83].

In such groups, we distinguish between *hard* and *soft* forms of exclusivity, the former assuming strict exclusivity among alterations, with random errors accounting for possible overlaps (i.e., the majority of samples do not share alterations from such groups), the latter admitting co-occurrences (i.e., some samples might have common alterations, within a group) [77].

CAPRI is currently the only algorithm which incorporates this type of information, in inferring a model. Each of these groups are in fact associated with a “*testable hypothesis*” written in the well-known language of *propositional Boolean formulas*⁵. Consider the following example: we might be informed that APC and CTNNB1 *mutations* show a trend of soft-exclusivity in our cohort – i.e., some samples harbor both mutations, but the majority just one of the two mutated genes. Since such mutations lead to β -catenin deregulation (the phenotype), we might wonder whether such state of affairs could be responsible for progression initiation in the tumors under study. An affirmative response would equate, in terms of progression, the two mutations. To *test this hypothesis*, one may spell out formula $APC \vee CTNNB1$ to CAPRI, which means that we are suggesting to the inference engine that, besides the possible evolutionary trajectories that might be inferred by looking at the two mutations as *independent*, trajectories involving such a “composite” event, shall be considered as well. It is then up to CAPRI to decide which, of all such trajectories, is significant, in a *statistical sense*.

In general, formulas allow users to test general hypotheses about complex model structures involving multiple genes and alterations. These are useful in many cases: for instance, where we are processing samples which harbour homozygous losses or inactivating mutations in certain genes (i.e., equally disruptive genomic events), or when we know in advance that certain genes are controlling the same pathway, and we might speculate that a single hit in one of those decreases the selection pressure on the others. We note that, with no hypothesis, a model with such alternative trajectories *cannot be analyzed, due to various computational limitations* inherent to the inferential algorithms (see [40]).

From a practical point of view, CAPRI’s formulas/hypotheses-testing features “help” the inference process, but do not “force” it to select a specific model, i.e., the *inference is not biased*. In this sense, the trajectories inferred by examining these composite model structures (i.e., the formulas) *are not given any statistical advantage* for inclusion in the final model. However, in spite of a natural temptation to generate as many hypotheses as possible, it is prudent to always limit the number of hypotheses according to the number of samples and alterations. Note that this approach can also be extended to accommodate, for instance, co-occurrent alterations in significantly mutated subnetworks [84, 85].

⁵There, logical connectives such as \oplus (the logical “xor”) act as a proxy for hard-exclusivity, and \vee (the logical “disjunction”) for soft one. Besides from exclusivity groups, other connectives such as logical conjunction can be used.

2.4 Progression inference and confidence estimation

We use CAPRI to reconstruct cancer progression models of each identified molecular subtype, provided that there exist a reasonable list of driver events and the groups of fitness-equivalent exclusive alterations. Since currently CAPRI represents the state of the art, and supports complex formulas for groups of alterations detected in the earlier PicNic step, it was well-suited for the task.

CAPRI’s input is a binary $n \times (m + k)$ matrix \mathbf{M} with n samples (a subtype size), m driver alteration events (0/1 Bernoulli random variables) and k testable formulas. Each sample in \mathbf{M} is described by a binary sequence: the 1’s denote the presence of alterations. CAPRI first performs a computationally fast *scan* of \mathbf{M} to identify a set \mathcal{S} of plausible selective advantage relations among the driver alterations and the formulas; then, it reduces \mathcal{S} to the most relevant ones, $\hat{\mathcal{S}} \subset \mathcal{S}$. Each relation is represented as an edge connecting drivers/formulas in a Graphical Model – which shall be termed Suppes-Bayes Causal Network. This network represents the *joint probability distribution*⁶ of observing a set of driver alterations in a cancer genome, subject to constraints imposed by Suppes’ *probabilistic causation* formalism [42].

Set \mathcal{S} is built by a statistical procedure. Among any pair of input drivers/formulas x and y , CAPRI postulates that $x \rightarrow y \in \mathcal{S}$ could be a selective advantage relation with “ x selecting for y ” if it estimates that two conditions hold

1. “ x is earlier than y ”;
2. “ x ’s presence increases the probability of observing y ”.

Such claims, grounded in Suppes’ theory of probabilistic causation, are expressed as inequalities over *marginal* and *conditional* distributions of x and y . These are assessed via a standard Mann-Whitney U test after the distributions are estimated from a reasonable number (e.g., 100) of *non-parametric bootstrap resamples* of \mathbf{M} (see Supplementary Material). CAPRI’s increased performance over existing methods can be motivated by the reduction of the state space within which models are searched, via \mathcal{S} .

Optimization of \mathcal{S} is central to our tolerance to *false positives* and *negatives* in $\hat{\mathcal{S}}$. We would like to select only the minimum number of relations which are true and statistically supported, and build our model from those. CAPRI’s implementation in TRONCO [41] selects a subset by optimizing a *score function* which assigns to a model a real number equal to its *log-likelihood* (probability of generating data for the model) minus a *penalty term* for model complexity – a regularization term increasing with $\hat{\mathcal{S}}$ ’s size, and hence penalizing overly complex models. It is a standard approach to avoid overfitting, and usually relies on the Akaike or the Bayesian Information Criterion (AIC or BIC) as regularizers. Both scores are approximately correct; AIC is more prone to overfitting but likely to provide also good predictions from data and is better when false negatives are more misleading than positive ones. BIC is more prone to underfitting errors, thus more parsimonious and better

⁶Technically, for a set of m alterations modeled by variables $\mathbf{x}_1, \dots, \mathbf{x}_m$, such a network is a Graphical Model representing the factorization of the joint distribution – $\mathcal{P}(\mathbf{x}_1, \dots, \mathbf{x}_m)$ – of observing any of the alterations in a genome (i.e., $\mathbf{x}_i = 1$). This factorization is made compact as the model encodes the statistical dependencies in its structure via

$$\mathcal{P}(\mathbf{x}_1, \dots, \mathbf{x}_m) = \prod_{i=1}^m \mathcal{P}(\mathbf{x}_i \mid \pi_i)$$

where $\pi_i = \{\mathbf{x}_j \mid \mathbf{x}_j \rightarrow \mathbf{x}_i \in \hat{\mathcal{S}}\}$ are the “parents” of the i -th node. These are those from which the presence of the i -th alteration is predicted. In our approach these edges are the pictorial representation of the selective advantage relations where the alterations in π_i select for \mathbf{x}_i .

in opposite direction. As often done, we suggest approaches that to combine but distinguish which relations are selected by BIC versus AIC. Details on the algorithm are provided as see Supplementary Material.

Statistical confidence of a model. In-vitro and in-vivo experiments provide the most convincing validation for the newly suggested selective advantage relations and hypotheses, yet this is out of reach in some cases.

Nonetheless, statistical validation approaches can be used almost universally to assess the confidence of edges, parent sets and whole models, either via *hypothesis-testing* or *bootstrap* and *cross-validation* scores for Graphical Models. We briefly discuss approaches that are implemented in TRONCO, and refer to the Supplementary Materials for additional details.

First, CAPRI builds \mathcal{S} by computing two p-values per edge, for the confidence in condition (1) and (2). In addition, for each edge $x \rightarrow y$, it computes a third p-value via hypergeometric testing against the hypothesis that the co-occurrence of x and y is due to chance. These p-values measure confidence in the direction of each edge and the amount of statistical dependence among x and y .

Second, for each model inferred with CAPRI we can estimate (*a posteriori*) how frequently our edges would be retrieved if we resample from our data (*non-parametric* bootstrap), or from the model itself, assuming its correctness (*parametric* bootstrap) [86]. Also, we can measure the bias in CAPRI’s construction of \mathcal{S} due to the random procedure which estimates the distributions in condition (1) and (2) (*statistical* bootstrap).

Third, scores can be computed to quantify the consistency for the model against bias in the data and models. For instance, *non-exhaustive* k -fold cross-validation can be used to compute the *entropy loss* for the whole model, and the *prediction* and *posterior classification errors* for each edge or parent set [87].

3 Results

3.1 Evolution in a population of MSI/MSS colorectal tumors.

It is common knowledge that *colorectal cancer* (CRC) is a heterogeneous disease comprising different molecular entities. Indeed, it is currently accepted that colon tumors can be classified according to their global genomic status into two main types: *microsatellite unstable tumors* (MSI), further classified as high or low, and *microsatellite stable* (MSS) tumors (also known as tumors with *chromosomal instability*). This taxonomy plays a significant role in determining pathologic, clinical and biological characteristics of CRC tumors [88]. Regarding molecular progression, it is also well established that each subtype arises from a distinctive molecular mechanism. While MSS tumors generally follow the classical adenoma-to-carcinoma progression described in the seminal work by Vogelstein and Fearon [89], MSI tumors result from the inactivation of DNA mismatch repair genes like MLH-1 [90].

With the aid of the TRONCO package, we instantiated PicNic to process colorectal tumors freely available through TCGA project COADREAD [56] (see Supplementary Figure S1), and inferred models for the MSS and MSI-HIGH tumor subtypes (shortly denoted MSI) annotated by the consortium. In doing so, we used a combination of background knowledge produced by TCGA and new computational predictions; to a different degree, some knowledge comes from manual curation of data and other from tools mentioned in PicNic’s description (see Figure 2). Data and exclusiv-

ity groups for MSI tumors are shown in Figure 3, the analogous for MSS tumors is provided as Supplementary Material.

For the models inferred, which are shown in Figures 4 and 5, we evaluated various forms of statistical confidence measured as p-values, bootstrap scores (in what follows, **npb** denotes non-parametric bootstrap and the closer to 100 the better), and cross-validation statistics reported in the Supplementary Material. Many of the postulated selective advantage relations (i.e., model edges) have very strong statistical support for COADREAD samples, although events with similar marginal frequency may lead to ambiguous imputed temporal ordering (i.e., the edge direction). In general, we observed that overall the estimates are slightly better in the MSS cohort (entropy loss < 1% versus 3.8%), which is expected given the difference in sample size of the two datasets (152 versus 27 samples), see Material and Methods for details.

Interpretation of the models. Our models capture the well-known features distinguishing MSS and MSI tumors: for the former APC, KRAS and TP53 mutations as primary events together with chromosomal aberrations, for the latter BRAF mutations and lack of chromosomal alterations. Of all 33 driver genes, 15 are common to both models - e.g., APC, BRAF, KRAS, NRAS, TP53 and FAM123B among others (mapped to pathways like WNT, MAPK, apoptosis or activation of T-cell lymphocytes), although in different relationships (position in the model), whereas new (previously un-implicated) genes stood out from our analysis and deserve further research.

MSS (Microsatellite Stable). In agreement with the known literature, in addition to KRAS, TP53 and APC as primary events, we identify PTEN as a late event in the carcinogenesis, as well as NRAS and KRAS converging in IGF2 amplification, the former being “selected by” TP53 mutations (**npb** 49%), the latter “selecting for” PIK3CA mutations (**npb** 81%). The leftmost portion of the model links many WNT genes, in agreement with the observation that multiple concurrent lesions affecting such pathway confer selective advantage. In this respect, our model predicts multiple routes for the selection of alterations in SOX9 gene, a transcription factor known to be active in colon mucosa [91]. Its mutations are directly selected by APC/CTNNB1 alterations (though with low **npb** score), by ARID1A (**npb** 34%) or by FBXW7 mutations (**npb** 49%), an early mutated gene that both directly, and in a redundant way via CTNNB1, relates to SOX9. The SOX family of transcription factors have emerged as modulators of canonical WNT/ β -catenin signaling in many disease contexts [92]. Also interestingly, FBXW7 has been previously reported to be involved in the malignant transformation from adenoma to carcinoma [93]. The rightmost part of the model involves genes from various pathways, and outlines the relation between KRAS and the PI3K pathway. We indeed find selection of PIK3CA mutations by KRAS ones, as well as selection of the whole MEMO module (**npb** 64%), which is responsible for the activation of the PI3K pathway [56]. SMAD4 proteins relate either to KRAS (**npb** 34%), and FAM123B (through ATM) and TCF7L2 converge in DKK2 or DKK4 (**npb** 81, 17 and 34%).

MSI-HIGH (Microsatellite Unstable). In agreement with the current literature, BRAF is the most commonly mutated gene in MSI tumors [94]. CAPRI predicted convergent evolution of tumors harbouring FBXW7 or APC mutations towards deletions/mutations of NRAS gene (**npb** 21, 28 and 54%), as well as selection of SMAD2 or SMAD4 mutations by FAM123B mutations (**npb** 23 and 46%), for these tumors. Relevant to all MSI tumors seems again the role of the PI3K pathway. Indeed, a relation among APC and PIK3CA mutations was inferred (**npb** 66%), consistent with recent experimental evidences pointing at a synergistic role of these

mutations, which co-occur in the majority of human colorectal cancers [95]. Similarly, we find consistently a selection trend among APC and the whole MEMO module (npb 48%). Interestingly, both mutations in APC and ERBB3 select for KRAS mutations (npb 51 and 27%), which might point to interesting therapeutic implications. In contrast, mutations in BRAF mostly select for mutations in ACVR1B (npb 36%), a receptor that once activated phosphorylates SMAD proteins. It forms receptor complex with ACVR2A, a gene mutated in these tumors that selects for TCF7L2 mutations (npb 34%). Tumors harbouring TP53 mutations are those selected by mutations in AXIN2 (npb 32%), a gene implicated in WNT signalling pathway, and related to unstable gastric cancer development [96]. Inactivating mutations in this gene are important, as it provides serrated adenomas with a mutator phenotype in the MSI tumorigenic pathway [97]. Thus, our results reinforce its putative role as driver gene in these tumors.

By comparing these models we can find similarity in the prediction of a potential new early event for CRC formation, FBXW7, as other authors have recently described [93]. This tumor suppressor is frequently inactivated in human cancers, yet the molecular mechanism by which it exerts its anti-tumor activity remains unexplained [98], and our models provide a new hypothesis in this respect.

4 Discussion

This paper represents our continued exploration of the nature of somatic evolution in cancer, and its translational exploitation through models of cancer progression, models of drug resistance (and efficacy), left- and right-censoring, sample stratification, and therapy design. Thus this paper emphasizes the engineering and dissemination of production-quality computational tools as well as validation of its applicability via use-cases carried out in collaboration with translational collaborators: e.g., colorectal cancer, analyzed jointly with epidemiologists currently studying the disease actively. As anticipated, we reasserted that the proposed model of somatic evolution in cancer not only supports the heterogeneity seen in tumor population, but also suggests a selectivity/causality relation that can be used in analyzing (epi)genomic data and exploited in therapy design – which we introduced in our earlier works [39, 40]. In this paper, we have introduced an open-source pipeline, PicNic, which minimizes the confounding effects arising from inter-tumor heterogeneity, and we have shown that PicNic can be effective in extracting ensemble-level evolutionary trajectories of cancer progression.

When applied to a highly-heterogeneous cancer such as colorectal, PicNic was able to infer the role of many known events in colorectal cancer progression (e.g., APC, KRAS or TP53 in MSS tumors, and BRAF in MSI ones), confirming the validity of our approach⁷. Interestingly, new players in CRC progression stand out from this analysis such as FBXW7 or AXIN2, which deserve further investigation. In colon carcinogenesis, although each model identifies characteristic early mutations suggesting different initiation events, both models appear to converge in common pathways and functions such as WNT or MAPK.

⁷As a further investigation for CRC, we leave as future work to check whether the inferred progression are also representative of other subtyping strategies for colorectal cancer, with particular reference to recent works which show marked interconnectivity between different independent classification systems coalescing into four consensus molecular subtypes [99].

However, both models have some clear distinctive features. Specific events in MSS include mutations in intracellular genes like CTNNB1 or in PTEN, a well-known tumor suppressor gene. On the contrary, specific mutations in MSI tumors appear in membrane receptors such as ACVR1B, ACVR2A, ERBB3, LRP5, TGFBR1 and TGFBR2, as well as in secreted proteins like IGF2, possibly suggesting that such tumors need to disturb cell-cell and/or cell-microenvironment communication to grow. At the pathway level, genes exclusively appearing in the MSI progression model accumulate in specific pathways such as cytokine-cytokine receptor, endocytosis and TGF- β signaling pathway. On the other hand, genes in MSS progression model are implicated in P53, mTOR, sodium transport or inositol phosphate metabolism.

Our study also highlighted the translational relevance of the models that we can produce with PicNic (see Supplementary Figure S12). The evolutionary trajectories depicted by our models can, for instance, suggest previously-uncharacterized phenotypes, help in finding biomarker molecules predicting cancer progression and therapy response, explain drug resistant phenotypes and predict metastatic outcomes. The logical structure of the formulas describing alterations with equivalent fitness (i.e., the exclusivity group) can also point to novel targets of therapeutic interventions. In fact, exclusivity groups that are found to have a role in the progression can be screened for *synthetic lethality* among such genes – thus explaining why we do not observe phenotypes where such alterations co-occur. In this sense, our models describe also such clonal signatures which, though theoretically possible, are not selected. We call such conspicuously absent phenotypes *anti-hallmarks* [100].

Our models have other applications to both computational and cancer research. Our models, as encoded by Suppes-Bayes Causal Networks could be used as informative *generative models* for the genomic profiles for the cancer patients. In fact, as known in machine learning, such generative models are extremely useful in creating better representation of data in terms of, e.g., discriminative kernels, such as Fisher [101]. In practice, this change of representations would allow framing common classification problems in the domain of our generative structures, i.e., the models, rather than the data. As a consequence, it is possible to create a new class of more robust classification and prediction systems.

One may think of these representations as those bringing us closer to phenotypic (and causal) representation of the patient’s tumor, replacing its genotypic (and mutational) representation. We suspect that such representations will improve the accuracy of measurement of the biological clocks, dysregulated in cancer and critically needed to be measured in order to predict survival time, time to metastasis, time to evolution of drug resistance, etc. We believe that these “phenotypic clocks” can be used immediately to direct the therapeutic intervention.

Clearly, applicability and reliability of techniques such as PicNic is very much dependent on the background of data available. At the time of this writing, the quality, quantity and reliability of (epi)genomic data available, e.g., in public databases, is related to the ever increasing computational and technological improvements characterizing the wide area of cancer genomics. Of similar importance is the availability of wet-lab technologies for models validation. Our recent work on SubOptical Mapping technology, for instance, points to the ability to cheaply and accurately characterize translocation, indels and epigenomic modifications at the single molecule and single cell level [102, 103]. This technology also provides the ability to directly validate (or refute) the hypotheses generated by PicNic via gene-correction and single cell perturbation approaches.

To conclude, the precision of any statistical inference technique, including PicNic, is influenced by the quality, availability and idiosyncrasies of the input data – the goodness of the outcomes improving along with the expected advancement in the field. Nevertheless, the strength of the

proposed approach lies in the efficacy in managing possibly noisy/ biased or insufficient data, and in proposing refutable hypotheses for experimental validation.

5 Materials and methods

Processing COADREAD samples with PiCnIc. We instantiated PicNic to process clinically annotated high MSI-HIGH and MSS colorectal tumors collected from The Cancer Genome Atlas project “Human Colon and Rectal Cancer” (COADREAD) [56] – see Supplementary Figure S1. Details on the implementation and the source code to replicate this study are available as Supplementary Material. COADREAD has enough samples, especially for MSS tumors, to implement a consistent and significant statistical validation of our findings – see Supplementary Table S1.

In brief, we split subtypes by the microsatellite status of each tumor as annotated by the consortium (so, step I of PicNic is done by exploiting background knowledge rather than computational predictors). It should be expected that if this step is skipped or this classification is incorrect, the resulting models would noticeably differ. Once split into groups, the input COADREAD data is processed to maintain only samples for which both high-quality curated mutation and CNA data are available; for CNAs we use focal high-level amplifications and homozygous deletions.

Then, for each sample we select only alterations (mutations/CNAs) from a list of 33 driver genes manually annotated to 5 pathways in [56] – WNT, RAF, TGF- β , PI3K and P53 (Supplementary Figures S2 and S3). This list of drivers, step II of PicNic, is produced by TCGA, as a result of manual curation and running MutSigCV.

In the next module of the pipeline, we fetch groups of exclusive alterations. We scanned these groups by using the MUTEX tool (Supplementary Table S2), and merged its results with the group that TCGA detected by using the MEMO tool, which involves mainly genes from the PI3K pathway. Knowledge on the potential exclusivity among genes in the WNT (APC, CTNNB1) and RAF (KRAS, NRAS, BRAF) pathways was exploited as well. Groups were then used to create CAPRI’s formulas; we also included hypotheses for genes which harbour mutations and homozygous deletions across different samples, see Supplementary Table S3. Data and exclusivity groups for MSS tumors are shown in Supplementary Figure S4 and S5.

CAPRI was run, as the last step of PicNic, on each subtype, by selecting recurrent alterations from the pool of 33 pathway genes and using both AIC/BIC regularizer. Timings to run the relevant steps of the pipeline are reported in the Supplementary Material. In the models of Figures 4 and Figure 5 each edge mirrors selective advantage among the upstream and downstream nodes, as estimated by CAPRI; Mann-Withney U test is carried out with statistical significance 0.05, after 100 non-parametric bootstrap iterations.

The significance of the reconstructed models and the input data is assessed by computing all the statistics/tests discussed in the Main text (temporal priority, probability raising and hypergeometric testing p-values, bootstrap and cross-validation scores). Motivation and background on each of these measures is available in the Supplementary Materials. A table with their values for edges with highest non-parametric bootstrap scores is in Supplementary Figure S8.

For the MSS cohort all the p-values are strongly significant ($p \ll 0.01$) except for the temporal priority of the edges connecting mutations in FAM123B and ATM, and ERBB2 alterations (mutations and amplifications), which leads us to conclude that, even if these pairs of genes seem to undergo selective advantage, the temporal ordering of their occurrence is ambiguous and failed to be imputed correctly from the datasets, analyzed here. The same situation occurs in MSI-HIGH tumors, for the relation between KRAS and ERBB3. Non-parametric and statistical bootstrap estimations are used

to assess the strength of all the findings (Supplementary Figures S6 and S7). Moreover, any bias in the data is finally evaluated by cross-validation (Supplementary Figures S8-S11) and common statistics such as entropy loss, posterior classification and prediction errors. In general, most of the selective advantage relations depicted by the inferred models present a strong statistical support, with the MSS cohort presenting the most reliable results.

Summary implementation for COADREAD (PicNic steps, Figure 2): (1) TCGA clinical classification, (2) MutSigCV and TCGA manual curation, (3) MEMO, MUTEX and knowledge of *wnt* and *raf* pathways and (4) CAPRI.

Implement your own case study with PiCnIc/TRONCO. TRONCO started as a project before PicNic, and is our effort at collecting, in a free R package, algorithms to infer progression models from genomic data. In its current version it offers the implementation of the CAPRI and CAPRESE algorithms, as well as a set of routines to pre-process genomic data. With the invention of PicNic, it started accommodating software routines to easily interface CAPRI and CAPRESE to some of the tools that we mention in Figure 2. In particular, in its current 2.0 version it supports input/output for the Matlab Network Based Stratification tool (NBS) and the Java MUTEX tool, as well as the possibility to fetch data available from the cBioPortal for Cancer Genomics (<http://cbioportal.org>), which provides a Web resource for exploring, visualizing, and analyzing multidimensional cancer genomics data.

We plan to extend TRONCO in the future to support other similar tools and become an integral part of daily laboratory routines, thus facilitating application of PiCnIc to additional use cases.

Authors contributions This work follows up on our earlier project initiated by BM and carried out by Milan-Bicocca and the Catalan Institute of Oncology, based on a framework discussed at the 2014 School on Cancer, Systems and Complexity (CSAC). PicNic was designed and constructed by MA’s Bioinformatics lab at University of Milan-Bicocca, within a project led and supervised by GC. GC, AG and DR designed the pipeline, and GC, DR and LDS coded and executed it. Data gathering and model interpretation was done by GC, LDS, DR, AG together with BM, VM and RSP. GM, MA, VM and BM provided overall organizational guidance and discussion. GC, AG, RSP and BM wrote the original draft of the paper, which all authors reviewed and revised in the final form. BM and MA are co-senior authors.

Acknowledgments MA, GM, GC, AG, DR acknowledge the SysBioNet project, a MIUR initiative for the Italian Roadmap of European Strategy Forum on Research Infrastructures (ESFRI) and Regione Lombardia (Italy) for the research projects RetroNet through the ASTIL Program [12-4-5148000-40]; U.A 053 and Network Enabled Drug Design project [ID14546A Rif SAL-7], Fondo Accordi Istituzionali 2009. BM acknowledges founding by the NSF grants CCF-0836649, CCF-0926166 and a NCI-PSOC grant. VM and RSP acknowledge the Instituto de Salud Carlos III supported by The European Regional Development Fund (ERDF) grants PI11-01439, PIE13/00022, the Spanish Association Against Cancer (AECC) Scientific Foundation, and the Catalan Government DURSI, grant 2014SGR647.

We wish to thank the anonymous reviewers for their help in improving the quality and rigor of the presentation.

References

- [1] Nowell PC (1976) The clonal evolution of tumor cell populations. *Science* 194:23–28.
- [2] Fidler IJ (1978) Tumor heterogeneity and the biology of cancer invasion and metastasis. *Cancer Research* 38:2651–2660.
- [3] Dexter DL, et al. (1978) Heterogeneity of tumor cells from a single mouse mammary tumor. *Cancer Research* 38:3174–3181.
- [4] Merlo LM, Pepper JW, Reid BJ, Maley CC (2006) Cancer as an evolutionary and ecological process. *Nature Reviews Cancer* 6:924–935.
- [5] Hanahan D, Weinberg RA (2000) The hallmarks of cancer. *Cell* 100:57–70.
- [6] Hanahan D, Weinberg RA (2011) Hallmarks of cancer: the next generation. *Cell* 144:646–674.
- [7] Huang S, Ernberg I, Kauffman S (2009) *Cancer attractors: a systems view of tumors from a gene network dynamics and developmental perspective* (Elsevier), No. 7, pp 869–876.
- [8] Futreal PA, et al. (2004) A census of human cancer genes. *Nature Reviews Cancer* 4:177–183.
- [9] Vogelstein B, et al. (2013) Cancer genome landscapes. *Science* 339:1546–1558.
- [10] Garraway LA, Lander ES (2013) Lessons from the cancer genome. *Cell* 153:17–37.
- [11] Zack TI, et al. (2013) Pan-cancer patterns of somatic copy number alteration. *Nature Genetics* 45:1134–1140.
- [12] Baylin SB, Jones PA (2011) A decade of exploring the cancer epigenome - biological and translational implications. *Nature Reviews Cancer* 11:726–734.
- [13] Weinberg R (2013) *The Biology of Cancer* (Garland Science).
- [14] Albini A, Sporn MB (2007) The tumour microenvironment as a target for chemoprevention. *Nature Reviews Cancer* 7:139–147.
- [15] Greaves M, Maley CC (2012) Clonal evolution in cancer. *Nature* 481:306–313.
- [16] Nowak MA, Michor F, Iwasa Y (2003) The linear process of somatic evolution. *Proceedings of the National Academy of Sciences* 100:14966–14969.
- [17] Vogelstein B, Kinzler KW (2004) Cancer genes and the pathways they control. *Nature Medicine* 10:789–799.
- [18] Nowak MA (2006) *Evolutionary Dynamics* (Harvard University Press).
- [19] Wood LD, et al. (2007) The genomic landscapes of human breast and colorectal cancers. *Science* 318:1108–1113.

- [20] Jones S, et al. (2008) Core signaling pathways in human pancreatic cancers revealed by global genomic analyses. *Science* 321:1801–1806.
- [21] Parsons DW, et al. (2008) An integrated genomic analysis of human glioblastoma multiforme. *Science* 321:1807–1812.
- [22] Fisher R, Pusztai L, Swanton C (2013) Cancer heterogeneity: implications for targeted therapeutics. *British Journal of Cancer* 108:479–485.
- [23] Curtis C, et al. (2012) The genomic and transcriptomic architecture of 2,000 breast tumours reveals novel subgroups. *Nature* 486:346–352.
- [24] Gerlinger M, et al. (2012) Intratumor heterogeneity and branched evolution revealed by multiregion sequencing. *The New England Journal of Medicine* 366:883–892.
- [25] (2015) The Cancer Genome Atlas (TCGA) <https://tcga-data.nci.nih.gov><https://tcga-data.nci.nih.gov>.
- [26] Navin N, et al. (2011) Tumour evolution inferred by single-cell sequencing. *Nature* 472:90–94.
- [27] Eberwine J, Sul JY, Bartfai T, Kim J (2014) The promise of single-cell sequencing. *Nature Methods* 11:25–27.
- [28] Beerenwinkel N, Schwarz RF, Gerstung M, Markowetz F (2015) Cancer evolution: mathematical models and computational inference. *Systematic biology* 64:e1–e25.
- [29] Ramchandani S, Bhattacharya SK, Cervoni N, Szyf M (1999) DNA methylation is a reversible biological signal. *Proceedings of the National Academy of Sciences* 96:6107–6112.
- [30] Vogelstein B, et al. (1988) Genetic alterations during colorectal-tumor development. *The New England Journal of Medicine* 319:525–532.
- [31] Desper R, et al. (1999) Inferring tree models for oncogenesis from comparative genome hybridization data. *Journal of Computational Biology* 6:37–51.
- [32] Desper R, et al. (2000) Distance-based reconstruction of tree models for oncogenesis. *Journal of Computational Biology* 7:789–803.
- [33] Szabo A, Boucher K (2002) Estimating an oncogenetic tree when false negatives and positives are present. *Mathematical Biosciences* 176:219–236.
- [34] Beerenwinkel N, et al. (2005) Learning multiple evolutionary pathways from cross-sectional data. *Journal of Computational Biology* 12:584–598.
- [35] Beerenwinkel N, Eriksson N, Sturmfels B (2007) Conjunctive Bayesian networks. *Bernoulli* pp 893–909.
- [36] Gerstung M, Baudis M, Moch H, Beerenwinkel N (2009) Quantifying cancer progression with conjunctive Bayesian networks. *Bioinformatics* 25:2809–2815.
- [37] Attolini CSO, et al. (2010) A mathematical framework to determine the temporal sequence of somatic genetic events in cancer. *Proceedings of the National Academy of Sciences* 107:17604–17609.

- [38] Misra N, Szczurek E, Vingron M (2014) Inferring the paths of somatic evolution in cancer. *Bioinformatics* 17:2456–2463.
- [39] Olde Loohuis L, et al. (2014) Inferring tree causal models of cancer progression with probability raising. *PLOS ONE* 9:e115570.
- [40] Ramazzotti D, et al. (2015) CAPRI: efficient inference of cancer progression models from cross-sectional data. *Bioinformatics* 31:3016–3026.
- [41] De Sano L, et al. (2016) TRONCO: an R package for the inference of cancer progression models from heterogeneous genomic data. *Bioinformatics*, 10.1093/bioinformatics/btw03510.1093/bioinformatics/btw035.
- [42] Suppes P (1970) *A Probabilistic Theory of Causality* (North-Holland Publishing Company Amsterdam).
- [43] Navin NE (2014) Cancer genomics: one cell at a time. *Genome Biology* 15:452.
- [44] Wang Y, et al. (2014) Clonal evolution in breast cancer revealed by single nucleus genome sequencing. *Nature* 512:155–160.
- [45] Gerlinger M, et al. (2014) Genomic architecture and evolution of clear cell renal cell carcinomas defined by multiregion sequencing. *Nature Genetics* 46:225–233.
- [46] Oesper L, Mahmood A, Raphael BJ (2013) THetA: inferring intra-tumor heterogeneity from high-throughput dna sequencing data. *Genome Biol* 14:R80.
- [47] Oesper L, Satas G, Raphael BJ (2014) Quantifying tumor heterogeneity in whole-genome and whole-exome sequencing data. *Bioinformatics* 30:3532–3540.
- [48] Miller CA, et al. (2014) SciClone: inferring clonal architecture and tracking the spatial and temporal patterns of tumor evolution. *PLOS Computational Biology* 8:e1003665.
- [49] Roth A, et al. (2014) PyClone: statistical inference of clonal population structure in cancer. *Nature Methods* 11:396–398.
- [50] Jiao W, Vembu S, Deshwar AG, Stein L, Morris Q (2014) Inferring clonal evolution of tumors from single nucleotide somatic mutations. *BMC Bioinformatics* 15:35.
- [51] Fischer A, Vázquez-García I, Illingworth CJ, Mustonen V (2014) High-definition reconstruction of clonal composition in cancer. *Cell Reports* 7:1740–1752.
- [52] Zare H, et al. (2014) Inferring clonal composition from multiple sections of a breast cancer. *PLOS Computational Biology* 7:e1003703.
- [53] Garvin T, et al. (2015) Interactive analysis and assessment of single-cell copy-number variations. *Nature methods* 12:1058–1060.
- [54] Malikic S, McPherson AW, Donmez N, Sahinalp CS (2015) Clonality inference in multiple tumor samples using phylogeny. *Bioinformatics* 31:1349–1356.
- [55] El-Kebir M, Oesper L, Acheson-Field H, Raphael BJ (2015) Reconstruction of clonal trees and tumor composition from multi-sample sequencing data. *Bioinformatics* 31:i62–i70.

- [56] The Cancer Genome Atlas Network, et al. (2012) Comprehensive molecular characterization of human colon and rectal cancer. *Nature* 487:330–337.
- [57] Network CGAR, et al. (2013) Genomic and epigenomic landscapes of adult de novo acute myeloid leukemia. *The New England Journal of Medicine* 368:2059.
- [58] Network CGAR, et al. (2013) Comprehensive molecular characterization of clear cell renal cell carcinoma. *Nature* 499:43–49.
- [59] Bennett JM, et al. (1976) Proposals for the classification of the acute leukaemias french-american-british (FAB) co-operative group. *British Journal of Haematology* 33:451–458.
- [60] Lu J, et al. (2005) MicroRNA expression profiles classify human cancers. *Nature* 435:834–838.
- [61] Gao Y, Church G (2005) Improving molecular cancer class discovery through sparse non-negative matrix factorization. *Bioinformatics* 21:3970–3975.
- [62] de Souto MC, Costa IG, de Araujo DS, Ludermitr TB, Schliep A (2008) Clustering cancer gene expression data: a comparative study. *BMC Bioinformatics* 9:497.
- [63] Network CGAR, et al. (2011) Integrated genomic analyses of ovarian carcinoma. *Nature* 474:609–615.
- [64] Konstantinopoulos PA, et al. (2010) Gene expression profile of BRCAness that correlates with responsiveness to chemotherapy and with outcome in patients with epithelial ovarian cancer. *Journal of Clinical Oncology* 28:3555–3561.
- [65] Reis-Filho JS, Pusztai L (2011) Gene expression profiling in breast cancer: classification, prognostication, and prediction. *The Lancet* 378:1812–1823.
- [66] Hofree M, Shen JP, Carter H, Gross A, Ideker T (2013) Network-based stratification of tumor mutations. *Nature Methods* 10:1108–1115.
- [67] Zhong X, Yang H, Zhao S, Shyr Y, Li B (2015) Network-based stratification analysis of 13 major cancer types using mutations in panels of cancer genes. *BMC Genomics* 16:S7.
- [68] Lawrence MS, et al. (2013) Mutational heterogeneity in cancer and the search for new cancer-associated genes. *Nature* 499:214–218.
- [69] Gonzalez-Perez A, Lopez-Bigas N (2012) Functional impact bias reveals cancer drivers. *Nucleic Acids Research* 40:e169.
- [70] Tamborero D, Gonzalez-Perez A, Lopez-Bigas N (2013) OncodriveCLUST: exploiting the positional clustering of somatic mutations to identify cancer genes. *Bioinformatics* 29:2238–2244.
- [71] Dees ND, et al. (2012) MuSiC: identifying mutational significance in cancer genomes. *Genome Research* 22:1589–1598.
- [72] Tamborero D, Lopez-Bigas N, Gonzalez-Perez A (2013) Oncodrive-CIS: a method to reveal likely driver genes based on the impact of their copy number changes on expression. *PLOS ONE* 8:e55489.

- [73] Gundem G, et al. (2010) IntOGen: integration and data mining of multidimensional oncogenic data. *Nature Methods* 7:92–93.
- [74] Yeang CH, McCormick F, Levine A (2008) Combinatorial patterns of somatic gene mutations in cancer. *The FASEB Journal* 22:2605–2622.
- [75] Miller CA, Settle SH, Sulman EP, Aldape KD, Milosavljevic A (2011) Discovering functional modules by identifying recurrent and mutually exclusive mutational patterns in tumors. *BMC Medical Genomics* 4:34.
- [76] Ciriello G, Cerami E, Sander C, Schultz N (2012) Mutual exclusivity analysis identifies oncogenic network modules. *Genome Research* 22:398–406.
- [77] Babur Ö, et al. (2015) Systematic identification of cancer driving signaling pathways based on mutual exclusivity of genomic alterations. *Genome Biology* 16.
- [78] Vandin F, Upfal E, Raphael BJ (2012) De novo discovery of mutated driver pathways in cancer. *Genome Research* 22:375–385.
- [79] Zhao J, Zhang S, Wu LY, Zhang XS (2012) Efficient methods for identifying mutated driver pathways in cancer. *Bioinformatics* 28:2940–2947.
- [80] Leiserson MD, Blokh D, Sharan R, Raphael BJ (2013) Simultaneous identification of multiple driver pathways in cancer. *PLOS Computational Biology* 5:e1003054.
- [81] Leiserson MDM, Wu HT, Vandin F, Raphael BJ (2015) CoMEt: a statistical approach to identify combinations of mutually exclusive alterations in cancer. *Genome Biology* 16:160.
- [82] Hua X, et al. (2015) MEGSA: A powerful and flexible framework for analyzing mutual exclusivity of tumor mutations. *bioRxiv* <http://dx.doi.org/10.1101/027474><http://dx.doi.org/10.1101/027474>.
- [83] Szczurek E, Beerenwinkel N (2014) Modeling mutual exclusivity of cancer mutations. *PLoS Computational Biology* 10.
- [84] Leiserson MD, et al. (2015) Pan-cancer network analysis identifies combinations of rare somatic mutations across pathways and protein complexes. *Nature Genetics* 47:106–114.
- [85] Vandin F, Upfal E, Raphael BJ (2011) Algorithms for detecting significantly mutated pathways in cancer. *Journal of Computational Biology* 18:507–522.
- [86] Efron B, Tibshirani RJ (1994) *An Introduction to the Bootstrap* (CRC press).
- [87] Koller D, Friedman N (2009) *Probabilistic Graphical Models: Principles and Techniques - Adaptive Computation and Machine Learning* (The MIT Press).
- [88] Ogino S, Goel A (2008) Molecular classification and correlates in colorectal cancer. *The Journal of Molecular Diagnostics* 10:13–27.
- [89] Fearon ER, Vogelstein B (1990) A genetic model for colorectal tumorigenesis. *Cell* 61:759–767.
- [90] Vilar E, Gruber SB (2010) Microsatellite instability in colorectal cancer - the stable evidence. *Nature reviews Clinical oncology* 7:153–162.

- [91] Abdel-Samad R, et al. (2011) MiniSOX9, a dominant-negative variant in colon cancer cells. *Oncogene* 30:2493–2503.
- [92] Kormish JD, Sinner D, Zorn AM (2010) Interactions between sox factors and wnt/ β -catenin signaling in development and disease. *Developmental Dynamics* 239:56–68.
- [93] Li L, et al. (2014) Sequential expression of miR-182 and miR-503 cooperatively targets FBXW7, contributing to the malignant transformation of colon adenoma to adenocarcinoma. *The Journal of Pathology* 234:488–501.
- [94] Kim JH, Kang GH (2014) Molecular and prognostic heterogeneity of microsatellite-unstable colorectal cancer. *World Journal of Gastroenterology* 20:4230.
- [95] Deming DA, et al. (2014) PIK3CA and APC mutations are synergistic in the development of intestinal cancers. *Oncogene* 33:2245–2254.
- [96] Kim MS, Kim SS, Ahn CH, Yoo NJ, Lee SH (2009) Frameshift mutations of Wnt pathway genes AXIN2 and TCF7L2 in gastric carcinomas with high microsatellite instability. *Human Pathology* 40:58–64.
- [97] Muto Y, et al. (2014) DNA methylation alterations of AXIN2 in serrated adenomas and colon carcinomas with microsatellite instability. *BMC Cancer* 14:466.
- [98] Zhan P, et al. (2015) FBXW7 negatively regulates ENO1 expression and function in colorectal cancer. *Laboratory Investigation* 9:995?1004.
- [99] Guinney J, et al. (2015) The consensus molecular subtypes of colorectal cancer. *Nature medicine*, in print.
- [100] Loohuis LO, Witzel A, Mishra B (2014) Cancer hybrid automata: model, beliefs and therapy. *Information and Computation* 236:68–86.
- [101] Korsunsky I (2016) Ph.D. thesis (New York University).
- [102] Reed J, et al. (2012) Identifying individual dna species in a complex mixture by precisely measuring the spacing between nicking restriction enzymes with atomic force microscope. *Journal of The Royal Society Interface* 9:2341–2350.
- [103] Sundstrom A, et al. (2012) Image analysis and length estimation of biomolecules using afm. *IEEE Transactions on Information Technology in Biomedicine* 16:1200–1207.

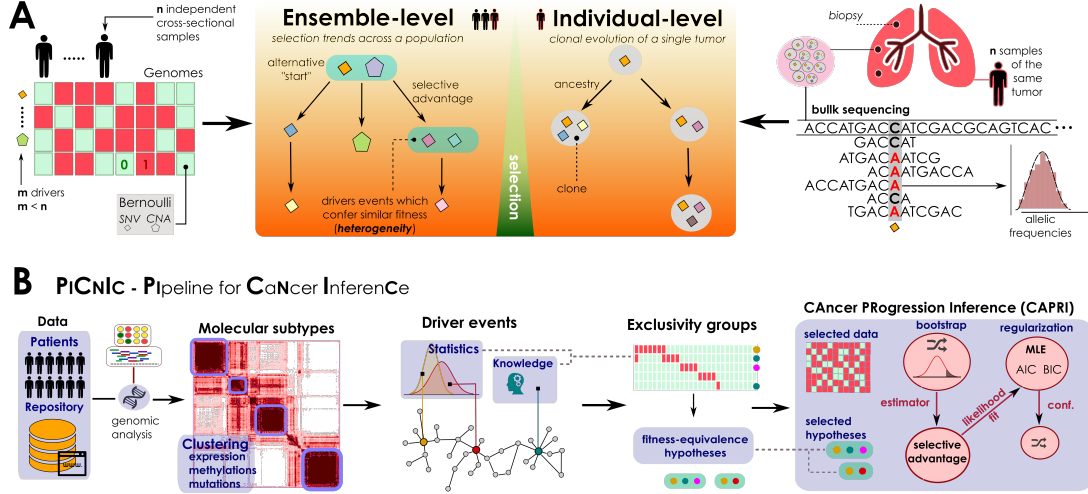


Figure 1: **A.** Problem statement. (left) Inference of ensemble-level cancer progression models from a cohort of n independent patients (cross-sectional). By examining a list of somatic mutations or CNAs per patient (0/1 variables) we infer a probabilistic graphical model of the temporal ordering of fixation and accumulation of such alterations in the input cohort. Sample size and tumor heterogeneity complicate the problem of extracting population-level trends, as this requires accounting for patients' specificities such as multiple starting events. (right) For an individual tumor, its clonal phylogeny and prevalence is usually inferred from multiple biopsies or single-cell sequencing data. Phylogeny-tree reconstruction from an underlying statistical model of reads coverage or depths estimates alterations' prevalence in each clone, as well as ancestry relations. This problem is mostly worsened by the high intra-tumor heterogeneity and sequencing issues. **B.** The PiCnIc pipeline for ensemble-level inference includes several sequential steps to reduce tumor heterogeneity, before applying the CAPRI [40] algorithm. Available mutation, expression or methylation data are first used to stratify patients into distinct tumor molecular subtypes, usually by exploiting clustering tools. Then, subtype-specific alterations driving cancer initiation and progression are identified with statistical tools and on the basis of prior knowledge. Next is the identification of the fitness-equivalent groups of mutually exclusive alterations across the input population, again done with computational tools or biological priors. Finally, CAPRI processes a set of relevant alterations within such groups. Via bootstrap and hypothesis-testing, CAPRI extracts a set of "selective advantage relations" among them, which is eventually narrowed down via maximum likelihood estimation with regularization (with various scores). The ensemble-level progression model is obtained by combining such relations in a graph, and its confidence is assessed via various bootstrap and cross-validation techniques.


		INPUT DATA *				COMPUTATIONAL OPTIONS AND PRIOR KNOWLEDGE ¶		EXPECTED OUTPUT AND ACTION TO EXECUTE	
	MOTIVATION	Mutations	Copy Number	Expression	Methylations	Other			
1	Cohort subtyping	Determine molecular subtypes likely to progress through different trajectories	✓	✓	✓		Non-negative Matrix Factorization (NMF), k-Means, Gaussian Mixtures, Hierarchical/Spectral Clustering, Network Based Stratification (NBS)	Biomarkers (cell types, known mutations, ...), Clinical Annotations (Mutation Status, Chromosomal Stability, ...)	Stratified samples (clusters) Split the cohort according to each cluster
2	Events selection	Select a subset of alterations likely to drive progression	✓	✓	✓		MutSigCV, OncodriveFM, OncodriveCLUST, MuSiC, Oncodrive-CIS, Intogen	Known cancer oncogenes and tumor suppressors, known pathways	A rank of genes and their alterations In each cluster, restrict to consider only driver events
3	Groups detection	Select groups of alterations which should be examined together	✓	✓	✓		Ratio test, RME, MEMO, MUTEX, Dendrix, MDPFinder, Multi-Dendrix, CoMEt, MEGSA, ME test	Known pathway genes with alternative but fitness-equivalent status, or co-occurently altered	Groups satisfying certain statistics (e.g., exclusivity) For each cluster, for each of its groups, create a logical formula consistent with the statistic
4	Model Inference	Select the Graphical Model which explains best the data	✓	✗	✗		CAPRI ★, CAPRESE, Oncotrees, Distance-based, Mixtures, CBN, Resic, BML		One progression model per subtype Validate statistically or experimentally each one of the inferred models
<small>* Data marked as ✗ can be used when it is persistent (i.e., do not revert back to their original state) during tumor progression. Other: data not common to most tumor types such as fusions or partial tandem duplication. ¶ Not all tools support all the data that is theoretically usable for a certain step. ★ CAPRI is the only algorithm to exploit knowledge provided by step 3 via logical formulas hypotheses-testing. Oncotrees, Distance-based, Mixtures and CAPRESE are constrained to infer at most tree-models of progression.</small>									

Figure 2: The PiCnIc pipeline. We do not provide a unique all-encompassing rationale to instantiate PiCnIc as all steps refer to research area currently development, where the optimal approach is often dependent on the type of data available and prior knowledge about the cancer under study. References are provided for each tool that can be used to instantiate PiCnIc: NMF [61], k-Means, Gaussian Mixtures, Hierarchical/Spectral Clustering [62], NBS [66], MutSigCV [68], OncodriveFM [69], OncodriveCLUST [70], MuSiC [71] Oncodrive-CIS [72] Intogen [73], Ratio [74], RME [75], MEMO [76], MUTEX [77], Dendrix [78], MDPFinder [79], Multi-Dendrix [80], CoMEt [81], MEGSA [82], ME [83], CAPRI [40], CAPRESE [39], Oncotrees [31, 33], Distance-based [32], Mixtures [34], CBN [35, 36], Resic [37] and BML [38].

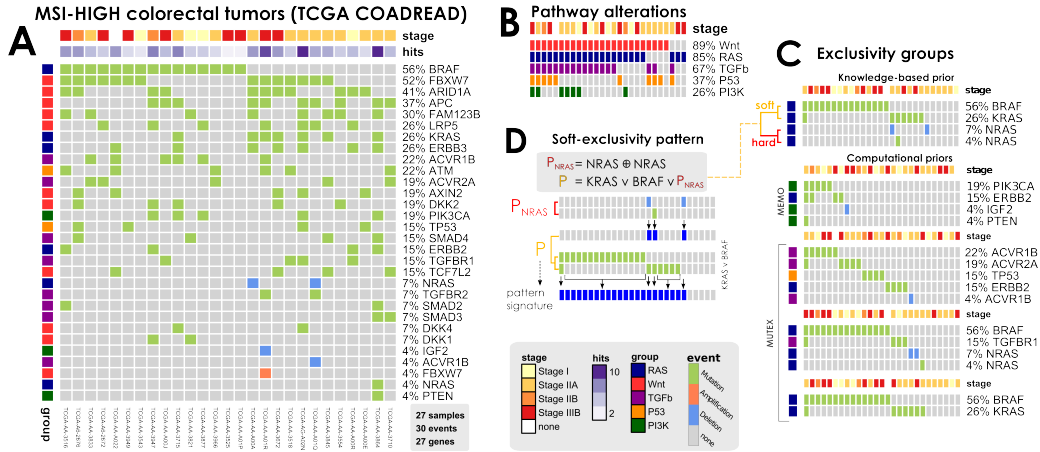


Figure 3: **A.** MSI-HIGH colorectal tumors from the TCGA COADREAD project [56], restricted to 27 samples with both somatic mutations and high-resolution CNA data available and a selection out of 33 driver genes annotated to WNT, RAS, PI3K, TGF- β and P53 pathways. This dataset is used to infer the model in Figure 5. **B.** Mutations and CNAs in MSI-HIGH tumors mapped to pathways confirm heterogeneity even at the pathway-level. **C.** Groups of mutually exclusive alterations were obtained from [56] - which run the MEMO [76] tool - and by MUTEX [77] tool. In addition, previous knowledge about exclusivity among genes in the RAS pathway was exploited. **D.** A Boolean formula input to CAPRI tests the hypothesis that alterations in the RAS genes KRAS, NRAS and BRAF confer equivalent selective advantage. The formula accounts for hard exclusivity of alterations in NRAS mutations and deletions, jointly with soft exclusivity with KRAS and NRAS alterations.

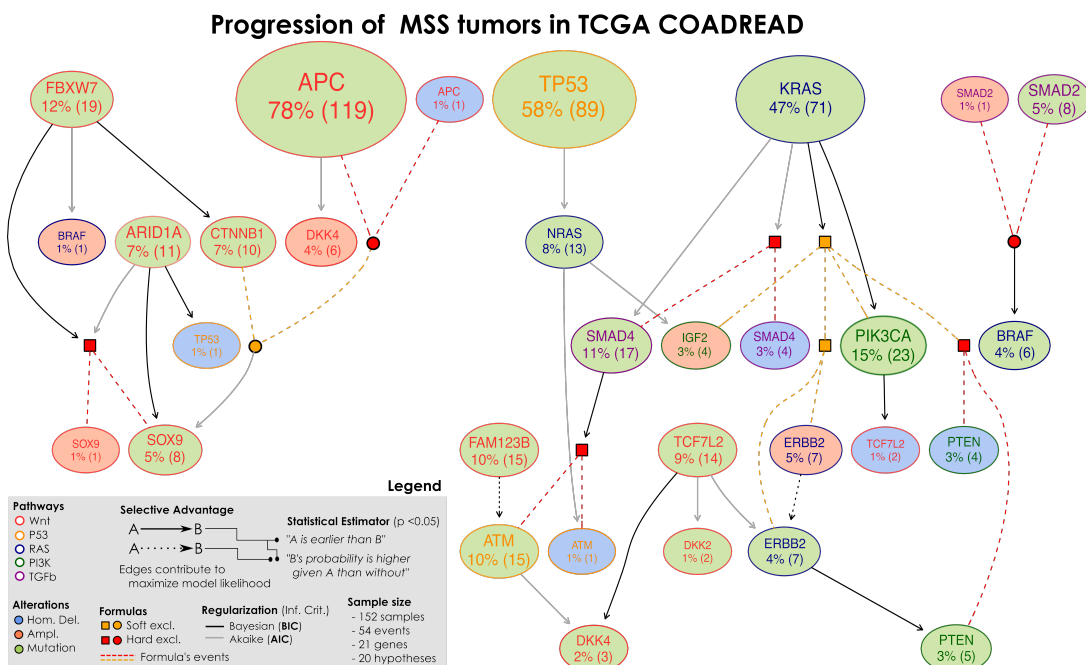


Figure 4: Selective advantage relations inferred by CAPRI constitute MSS progression; input dataset in Supplementary Figure S3 and S4. Formulas written on groups of exclusive alterations, e.g., SOX9 amplifications and mutations, are displayed in expanded form; their events are connected by dashed lines with colors representing the type of exclusivity (red for hard, orange for soft), logical connectives are squared when the formula is selected, and circular when the formula selects for a downstream node. For this model of MSS tumors in COADREAD, we find strong statistical support for many edges (p-values, bootstrap scores and cross-validation statistics shown as Supplementary Material), as well as the overall model. This model captures both current knowledge about CRC progression – e.g, selection of alterations in PI3K genes by the KRAS mutations (directed or via the MEMO group, with BIC) – as well as novel interesting testable hypotheses – e.g., selection of SOX9 alterations by FBXW7 mutations (with BIC).

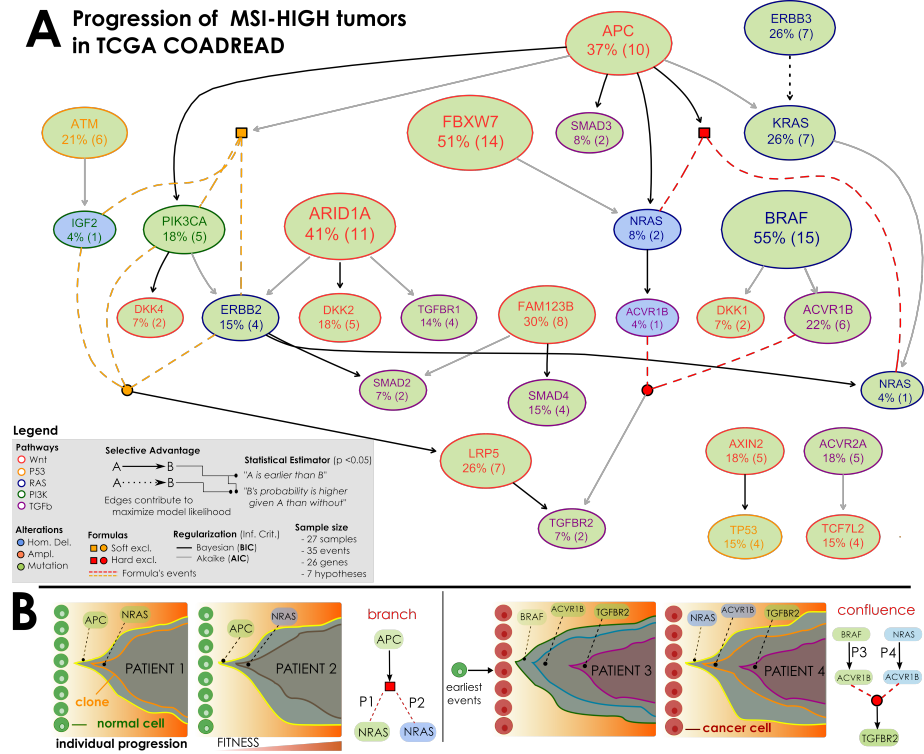


Figure 5: **A.** Selective advantage relations inferred by CAPRI constitute MSI-HIGH progression; input dataset in Figure 3. Formulas written on groups of exclusive alterations are expanded as in Figure 4. For each relation, confidence is estimated as for MSS tumors and reported as Supplementary Material. In general, this model is supported by weaker statistics than MSS tumors – possibly because of this small sample size ($n=27$). Still, we can find interesting relations involving APC mutations which select for PIK3CA ones (via BIC) as well as selection of the MEMO group (ERBB2/PIK3CA mutations or IGF2 deletions) predicted by AIC. Similarly, we find a strong selection trend among mutations in ERBB2 and KRAS, despite in this case the temporal precedence among those mutations is not disentangled as the two events have the same marginal frequencies (26%). **B.** Evolutionary trajectories of clonal expansion predicted from two selective advantage relations in the model. APC-mutated clones shall enjoy expansion, up to acquisition of further selective advantage via mutations or homozygous deletions in NRAS. These cases should be representative of different individuals in the population, and the ensemble-level interpretation should be that “APC mutations select for NRAS alterations, in hard exclusivity” as no sample harbour both alterations. A similar argument can show that the clones of patients harbouring distinct alterations in ACVR1B – and different upstream events – will enjoy further selective advantage from mutation in the TGFBR2 gene.

A Reproducing this study

Code availability

The implementation of PiCnIc shown in the Main Text was performed by using, as core, the R language, and other external Java tools which we reference in this document. In R, much of the data processing and inference is done by exploiting the current version of the open-source

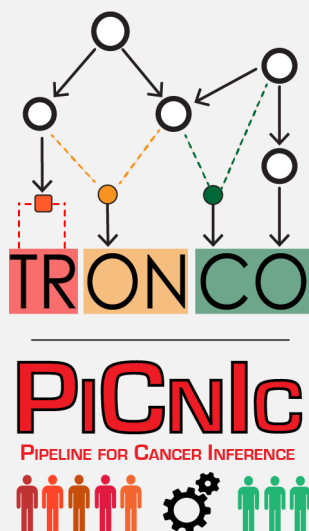
TRanslational **ONCO**logy (TRONCO, [41], version 2.3)

package which implements up-to-date statistical algorithms to estimate cancer progression models from a list of genomic lesions (e.g., somatic mutations, copy number variations or persistent epigenetic states) in a population of independent tumors, or in a single patient.

TRONCO's official webpage is reachable from the Software section of our group's webpage

<http://bimib.disco.unimib.it/>

By navigating to the Case Studies section of TRONCO's official webpage one can find the source code to replicate this study (i.e., the PicNic's implementation) along with the documentation detailing all the implementation, as well as the data that we used. This should allow easy implementation of similar studies in different contexts.



B Glossary

This glossary of terms shall be of help to readers not familiar with the concepts mentioned in the Main Text. For clarity, terms are separate in two categories according to the fact that they are common to the statistics or the cancer biology communities. Each term which is included in this glossary appears in color.

Terms common to the statistics community

Term	Meaning
Boolean formula	In CAPRI, a formula written with standard logical operators which capture a relation among a group of alterations. In PicNic, these are used to detect alternative routes to selective advantage from mutually exclusive alterations . See: Fitness equivalence .
Ensemble level progression inference	Detection of the relations of selective advantage across the permanent alterations in a cohort of independent tumors (cross-sectional data). When aggregated in a graphical model , these shall picture the most common evolutionary trajectories in the population/cancer under study. See also: inter-tumor heterogeneity .
Graphical models	In this context, a direct acyclic graph with nodes (alterations) and edges (selective advantage relations), as a shorthand to represent the joint probability of observing a set of alterations in a sample (i.e., a cancer genotype). See also: Suppes-Bayes Causal Network , Model selection .
Individual level progression inference	Detection of clonal signatures and their prevalence in individual tumors by scanning multi-region or single-cell sequencing data; clones are then displayed in a phylogenetic tree structure . See also: intra-tumor heterogeneity .
Model selection	The process of selecting a model which fits data, according to some criterion. In CAPRI, this is done by balancing model likelihood (a measure of to which degree data can be explained by the model) and model complexity (the size of the graphical model). See: regularization .
Phylogenetic tree	In this context, rooted tree where each node is a clone , and edges represent ancestry relations among clones.
Regularization	Common approach to avoid overfitting (false-positives) during model selection – in CAPRI this is achieved by using the standard AIC/BIC which penalize with different severity graphical models which contain many selective advantage relations .
Simposon's paradox	A paradox in statistics, in which a trend appears in different groups of data but disappears or reverses when these groups are combined. In this context, this shall refer to genuine selective advantage relations which are not inferred unless data coming from different populations is separated before doing inference. See: heterogeneity , subtypes , formulas .
Suppes-Bayes Causal Networks	A specific type of graphical model returned by CAPRI algorithm, where each edge satisfies Suppes's conditions of probabilistic causation subsuming temporal ordering and positive statistical dependence – the statistical approach to estimate selective advantage among the alterations.

Terms common to the cancer biology community

Term	Meaning
Alterations	Somatic mutations: A change in the genome of a cell that is not inherited from a parent, but is acquired. CNVs: Structural variation of large regions of DNA segments, including deletions, insertions, duplications and complex multi-site variants.
Bulk sequencing	Genome sequencing from single tumor samples, each containing a large number of cells. The resulting genomic profiles are derived from a mixture of cells with potentially distinct evolutionary histories.
Clones; Clonal expansion	Clone: group of cells sharing an identical genome and that derive from a common ancestor. Clonal expansion: the production of descendent cells all arising originally from a single cell. In the scenario of cancer development, tumors develop through a series of clonal expansions, in which the most favorable clonal population survives and proliferate.
Cross-sectional data	Unique snapshots of data derived from samples that are collected at unknown time points. Usually derived from bulk sequencing technologies.
Driver; Passenger	Driver: (epi)genetic alteration that provides a selective advantage to a cancer clone . Passenger: alteration of a cancer cell that does not increase its fitness .
Exclusivity of alterations	Group of alterations which manifest few or no co-occurrences in a cohort of different samples, and might be fitness-equivalent for tumor progression. Hard exclusivity: when co-occurrences shall be considered the result of random errors. Soft exclusivity: when few co-occurrences shall be possible. See: formulas .
Fitness	A cell's ability of surviving, proliferating and adapting to environmental changes, usually within an environment with limited and depleting resources (e.g., oxygen or nutrients).
Fitness equivalence	Groups of driver alterations , functional to the same pathway or equally disruptive, that can independently confer a selective advantage to a cancer cell. Multiple co-occurrence of such alterations to provide no further advantage, hence leading to mutually exclusive alteration patterns across distinct samples.
Hallmark of cancer	Common traits or phenotypic properties that are supposed to drive the transformation of normal cells to cancer cells. Anti-hallmark: clonal profiles that are usually not observed, yet being theoretically possible.
Inter-tumor heterogeneity	The phenomenon according to which different patients with the same cancer type usually display a few common alterations. This is the major problem of inferring ensemble-level cancer progression models .
Intra-tumor heterogeneity	Intra-tumor heterogeneity is related to possible coexistence of different cancer clones, with different evolutionary histories and different mutational profiles, within the same tumor. This is the major problem of inferring individual-level cancer progression models .
Multiregion sequencing	Collection of genomic data obtained by processing multiple spatially separated biopsy samples from the same individual tumor.
Next Generation Sequencing (NGS)	New technologies for sequencing genomes at high speed and low cost, including, e.g., full-genome/exome sequencing, genome resequencing, transcriptome profiling (RNA-Seq), DNA-protein interactions (ChIP-Seq), and epigenome characterization.
Selective advantage relation	In successive waves of clonal expansions one or more cells of the same clone can (progressively) increase their fitness through the acquisition of additional driver alterations , leading to the emergence and development of a fitter clone. In this case a relation of selective advantage connects the earlier to the succeeding alterations .
Single-cell sequencing	Recent technology based on the retrieval and analysis of genomic information from individual cells, rather than from mixtures of cells.
Synthetic lethality	The phenomenon according to which two otherwise non-lethal alterations lead the cell death when they co-occur within the same cell. See: Anti-hallmark

C PicNic’s implementation for COADREAD samples

Here we detail all the steps implemented to use PicNic for CRC progression inference.

C.1 TCGA COADREAD project data

COADREAD provides genome-scale analysis of samples with exome sequence, DNA copy number, promoter methylation, messenger RNA and microRNA expression data, which we used to define the input dataset. In particular, only samples with both mutations and CNAs profiles were used in the analysis. Supplementary Table S1 details the dataset.

Dataset used to infer models presented in the Main Text. Samples published in [56] were used as, to the best of our knowledge, these represent the highest-quality data made available by COADREAD as of today; for these samples TCGA provides somatic mutation profiles and high-resolution focal CNAs via GISTIC. These are obtained from TCGA data freeze as of 2 February 2012, downloaded on 12 March 2015, from repository:

https://tcga-data.nci.nih.gov/docs/publications/coadread_2012/

The following files were processed to produce the data:

- `TCGA_CRC_Suppl_Table2_Mutations_20120719.xlsx`
Somatic mutations profiles obtained via whole-exome sequencing of 224 colorectal tumors by TCGA. Data available consists of 15995 mutations in 228 samples, provided in the *Manual Annotation Format* (MAF). Samples were selected to univocally match the 224 patients as of the TCGA guidelines for aliquote disambiguation, see <https://wiki.nci.nih.gov/display/TCGA/TCGA+barcode>. All the mutations annotated by TCGA – truncating (De_novo_Start_OutOfFrame, Frame_Shift_Del, Frame_Shift_In, Nonsense_Mutation, Splice_Site, Frame_Shift_Ins, In_Frame_Del), silent (Silent) and missense (Missense_Mutation) – were considered for analysis; notice that the majority of them are missense, see Figures S7 and S8.
- `crc_gistic.txt.zip`
Focal *Copy Number Alterations* (CNAs) for 564 patients derived from whole-genome sequencing using the Illumina HiSeq platform. *High-level gains* and *homozygous deletions* were considered for analysis by selecting entries with GISTIC scores ± 2 ;
- `crc_clinical_sheet.txt`
Clinical data summary with patient stage and *Micro Satellite Stable/Unstable* (MSS/MSI) status being any of: MSS, MSI-high and MSI-low.

The list of patients used was first reduced to those having *both* CNAs and somatic mutation data, and then was split into two groups: MSI-HIGH and MSS. The training cohort has 152 MSS and 27 MSI-HIGH samples; samples flagged as low MSI were excluded from the study as they have not been shown to differ in their clinicopathologic features or in most molecular features from MSS tumors [?].

C.2 Driver events selection

In the TCGA COADREAD study [56] integrated analysis of mutations, copy number and mRNA expression changes in 195 tumours with complete data was performed. Part of the analysis was carried out by using the MutSig tool [68], as well as manual curation. Samples were grouped by mutation status, and recurrent alterations in key CRC pathways were identified in [56] (Fig. 4, Supplementary Fig. 6 and Supplementary Table 1) as a result, we can use the consortium’s list of 33 driver genes annotated to 5 pathways and use these to extract our progression models. These are well-known cancer genes, frequently reported as relevant to colorectal progression and to the major pathways involved in CRC. Driver events are alterations in:

- WNT genes (14): APC, DKK-4, TCF7L2, CTNNB1, LRP5, FBXW7, DKK-1, FZD10, ARID1A, DKK-2, FAM123B, SOX9, DKK-3 and AXIN2;
- RTK/RAS genes (5): ERBB2, ERBB3, NRAS, KRAS and BRAF;
- TGF- β genes (5): TGFBR1, SMAD3, TGFBR2, SMAD4, ACVR1B, ACVR2A and SMAD2;
- IGF2/PI3K genes (5): IGF2, IRS2, PIK3CA, PIK3R1 and PTEN;
- P53 genes (2): TP53 and ATM.

In the Main Text, RTK/RAS and IGF2/PI3K pathways are shortly denoted as RAS and PI3K.

The distinct types of mutations detected in these genes are shown in Figure S7, as well as the overall rate of COADREAD mutations. The spatial distribution (per gene) of such mutations is shown in Figure S8.

C.3 Mutual exclusivity groups of alterations.

Groups of alterations showing a trend of mutual exclusivity were scanned with MUTEX and mutations and CNA hitting any of the 33 selected genes as input. MUTEX was run independently on MSS and MSI-HIGH groups (Supplementary Table S2, running times: approximately 6 and 3.5 hours, respectively, on a standard Desktop machine).

We selected only groups with score < 0.2 , where the score is derived from *p-values corrected for false discovery rate*. 3 groups are found for MSI-HIGH tumors and 6 for MSS. For MSI-HIGH tumors, the three predicted groups consists of genes ACVR1B, ACVR2A, TP53 and ERBB2, of genes BRAF, NRAS and TGFBR2, and of genes KRAS and BRAF.

Further groups of exclusive alterations were considered consistent with results reported in [56]. These include groups derived by consolidated knowledge of colorectal progression: the well-known WNT alterations in APC/CTNNB1 [?], as well as RAS alterations in KRAS, NRAS and BRAF genes [74]. Similarly, we used also a group collected by scanning non-hypermutated tumors with the MEMO tool in [56] - this group includes PIK3CA, PTEN, ERBB2 and IGF2 genes. These groups were restricted to account only for genes actually altered in a certain subtype, e.g., MSI-HIGH tumors lack CTNNB1 mutation, making the Wnt group irrelevant. Groups for MSS tumors are shown as Supplementary Figure S9, groups for MSI-HIGH tumors are in the Main Text.

C.4 CAPRI’s execution

Background on the algorithm. CAPRI algorithm can be executed in two different modes, originally dubbed as “supervised” when formulas are given in input for testing, and “unsupervised” when this is not the case. This paper deals with the former; see the Main Text for the interpretation of formulas in this context and [40] for a derivation of the algorithm. CAPRI is a three-steps procedure, which we briefly recall here.

1. CAPRI starts by creating a “lifted” representation of the input data \mathbf{M} which includes the input formulas; each formula – which is written in propositional logic – is so evaluated to yield a new column in the dataset. This is the input processed by the algorithm, which starts by selecting a set of candidate model edges, which are then used to constrain a score-based Bayesian model-selection problem [40].
2. The initial set of selective advantage relations \mathcal{S} , which determines the model edges $x \rightarrow y$, is computed by evaluating the following inequalities

$$\begin{aligned} \text{(Temporal priority)} \quad & p(x) > p(y) \\ \text{(Probability raising)} \quad & p(y \mid x) > p(y \mid \neg x), \end{aligned}$$

where $p(\cdot)$ is a marginal probability, $p(\cdot \mid \cdot)$ is a conditional, $\neg x$ is the negation of x and either x or y is not a formula. It is interesting to observe that **probability raising** implies that x and y are *positively statistically dependent*, thus imposing a minimum threshold on their association [39].

In each of CAPRI’s executions, the distribution of the observed marginals and conditionals are estimated by K non-parametric bootstrap resamples; practically, this means that we create a bootstrapped approximation for each of the four populations $\hat{p}(x)$, $\hat{p}(y)$, $\hat{p}(y \mid x)$ and $\hat{p}(y \mid \neg x)$. Then, we use a single-tail non-parametric Mann-Whitney U test of the difference in mean to test the hypothesis that one of the two populations is more probable than the other, e.g., $\hat{p}(x) > \hat{p}(y)$. With this test, we can compute two p-values, one for each condition. An edge is included in \mathcal{S} if at least the p-value for **probability raising** is below a significance threshold p_* and an edge is said not to be orientable if its p-value for **temporal priority** is above the same threshold. Cycles $x_1 \rightarrow x_2 \rightarrow \dots x_k \rightarrow x_1$ that might appear in \mathcal{S} are broken by deleting the edge with minimum p-value; both K and p_* are custom parameters.

3. Optimization of \mathcal{S} , namely detection of the subset \mathcal{S}^* of \mathcal{S} with the edges that we include in the final progression model is done by optimizing, via *hill climbing* or *tabu search*, the *score with regularization*

$$\mathcal{S}^* \triangleq \arg \min_{\hat{\mathcal{S}} \subset \mathcal{S}} \left\{ -2 \log[\mathcal{L}(\hat{\mathcal{S}} \mid \mathbf{M})] + \theta |\hat{\mathcal{S}}| \right\}, \quad (1)$$

where $\mathcal{L}(\cdot)$ is the *model likelihood* and \mathbf{M} is the input data; the estimated optimal solution is \mathcal{S}^* , which is displayed as a Suppes-Bayes Causal Network. The different regularization strategies mentioned in the Main Text, BIC and AIC, are obtained by the following parametrization:

$$\begin{aligned} \text{(Bayesian Information Criterion)} \quad & \theta \triangleq \log(n) \\ \text{(Akaike Information Criterion)} \quad & \theta \triangleq 2. \end{aligned}$$

Besides edges, a model has a set of parameters θ which define the *conditional probability table* of each edge and should be fit from data; these are necessary if one wishes to use a model as a “generator” of further data. For discrete-valued graphical models, for each parent set $\pi_x \rightarrow y$, parameter $\theta(y) = p(y | \pi_x)$ can be taken either as the *maximum likelihood estimate* from the lifted input, or by using a Bayesian interpretation [87].

Usage in this context. CAPRI was run, on each group of tumors, by selecting alterations from the pool of 33 pathway genes; every alteration on a gene x is included if *any* of these apply:

- the alteration frequency of x - sum of mutation and CNA frequency - is greater than 5%;
- x it is part of an exclusivity group.

The set of selected events for MSI-HIGH training tumors is shown in the Main Text, the analogous set for MSS tumors is shown as Supplementary Figure S10.

CAPRI was executed in its supervised mode by writing formula over groups and genes with multiple alterations associated, as explained in the Main Text. For instance, for MSI-HIGH tumors with alterations in RAS pathway we grouped hard exclusivity of NRAS mutations and deletions, with soft exclusivity of KRAS and BRAF mutations. Our aim was to account for a small subset of samples with concurrent KRAS and NRAS alterations (see Figure 2, Main Text). The list of all Boolean formulas written over groups is in Table S3; this approach was adopted also when a gene harbors multiple alterations in a subtype, e.g., ERBB2 in MSS training samples which shows a trend of soft exclusivity between mutations and amplifications. We used both AIC and BIC scores to regularize inference after 100 non-parametric bootstrap iterations for estimation of the preliminary selective advantage relations – Mann-Whitney U test was performed with a minimum threshold $p_* = 0.05$. In most cases p-values are orders of magnitude below p_* - exact values reported as Dataset File S1. CAPRI’s models with such p-values and non-parametric bootstrap confidence are shown in Figures S11 and S12, statistical validation of the models is discussed in the next section.

D Statistical validation of the models

P-values from hypothesis testing, as well as scores from k -fold *cross-validation* and various *bootstrapping* techniques can be used to measure the statistical consistency of models and data, each one capturing different potential errors in the inference process. Approaches such as cross-validation and bootstrap are sometimes also used in the (*ex novo*) generation and inference of models from data (see, e.g., *bootstrap consensus models* [?]), but we only use them here for the *a posteriori* evaluation of a model’s confidence, and we interpret them as a quantitative measure for the *relative* assessment of each model’s relation.

All the p-values and the scores that we present here are computed within TRONCO.

D.1 Edge p-values

As explained in §C.4, for each model edge $x \rightarrow y$ we get two p-values by assessing temporal priority and probability raising via Mann-Whitney U testing.

For each edge, a p-value for the *hypergeometric test* of overlap between alteration profiles x and y can be computed. More precisely, we test if there is a difference between the number of samples containing *both* x and y versus the total population of samples with x , y , or both. We would like

the overlap to be significant as those samples – that determine the joint probability of x and y – are those supporting the presence of a selection trend among x and y .

An edge is fully supported if all three p-values are below a custom significance threshold, e.g., 0.05 or even better 0.01. Some edges might have the p-value for temporal priority above the threshold. If so, the selection trend might be still significant, but the temporal order of x and y – i.e., the *direction of selection* – is not supported by the data.

D.2 Bootstrap

We used non-parametric and statistical bootstrap techniques to measure the *goodness-of-fit*, as originally proposed in [?]. In this case, we distinguish two type of errors that one could make in the inference process, estimating the presence or absence of edges in the model:

- *Type I errors*: incorrect rejection of a true H_0 (null-hypothesis), i.e., a “false positive” edge that we wrongly include.
- *Type II errors*: incorrect acceptance (failure to reject) of a false H_0 , i.e., a “false negative” edge that we miss.

Non-parametric bootstrap [86] computes scores to be interpreted here as follows. If a model contains an edge $x \rightarrow y$ that is a true positive, we expect its score to be high. In other words, when we sample with repetition subsets of the original data and re-run the inference process we expect to often find models which contain the edge $x \rightarrow y$. Conversely, for a node y without incoming edges, or equivalently for any edge $x \rightarrow y$ which is correctly excluded from a model – a true negative – we would expect its bootstrap score to be low. However, this reasoning can be also generalized to whole models, where we count how many times we re-infer exactly the same model. Clearly, such scores will depend also on the empirical probabilities of the nodes in our data, and their deviation from the true probabilities of the phenomenon. So, one might expect rare events to be less frequently bootstrapped, which results in a lower estimate; however, such counts can be anyway interpreted as measures of repeatability of our findings⁸.

The above bootstrap approach depends on two random number generators: one to shuffle data (the a posteriori bootstrap), and one to evaluate CAPRI’s inequalities via hypothesis testing (the internal CAPRI’s bootstrap, see C.4). Thus, to ensure that no bias is introduced by the random number generators, we performed a *statistical bootstrap* by holding data fixed, and re-estimating CAPRI’s inequalities with generators initialized with different seeds. We evaluated the robustness of our scores for all edges imputed to be genuine and hence, high-scoring.

Notice that, in principle, even *parametric bootstrap* scores could be computed if we used the model to generate bootstrapped data [86]. However, as the support of the distribution subsumed by a model with n nodes consists of 2^n possible outcomes, sampling uniformly from large models might be computationally hard. For this reason, and because such scores are overestimates of the non-parametric ones, we did not include them in our computation.

The MSS and MSI progression models are annotated with the non-parametric bootstrap scores in Figures S11 and S12. Non-parametric and statistical bootstrap scores for a set of selected edges

⁸Bootstrapping techniques have been widely used to gauge uncertainty in estimates, but also subjects of philosophical debate about their precise interpretation, especially when coupled with various significance thresholds – unlike the situation with a p-value for a null hypothesis. An exhaustive review on the topic is provided by Soltis in [?]. We follow the ideas originally developed in the area of phylogenetic analysis [?], suggesting that the scores can be alternatively interpreted as a measure of accuracy of the method or of the robustness of the data [?].

are shown and commented in Figure S13. For the same set of edges, we also report the p-values for CAPRI’s inequalities assessed in the MSS and MSI progression models (temporal priority and probability raising, as a measure of the selectivity among the alterations, and hypergeometric, as a measure of the randomness in the overlap of two alteration profiles). Additional comments are in the caption.

D.3 Cross-validation

Next we study the sufficiency of the data sizes for model inference and its ability to characterize the underlying progression (*goodness-of-data*). Thus, we focus on the Type III errors, which occur when the sample size is inadequate or the sample is a poor descriptor for the reference phenomenon⁹, and thus failing to represent the progression. For this purpose, we used cross-validation with the data used for the models built (see the Main Text), and followed the best practices developed by the Bayesian Networks community [87].

TRONCO exploits the cross-validation routines implemented in the `bnlearn` package [?]. The approach that we adopt is a k -fold non-exhaustive cross-validation, which we repeat 10 times to average its results. Exhaustive strategies might be used for datasets of small sample size. Each run of cross-validation consists in computing a loss function for a model; its steps are the followings:

- split randomly the data in $k = 10$ groups, and then repeat the following two steps, for each group in turn:
 1. set one of the groups to be the “training” \mathbf{M}_{tr} ;
 2. merge the others $k - 1$ to be the “test” \mathbf{M}_{te} ;
 3. by holding fixed the model structure (i.e., the edges in \mathcal{S}^*), fit the model parameters θ over the training data via *maximum likelihood estimates*, compute a score over the test \mathbf{M}_{te} (see below) and the corresponding loss;
- combine the k loss estimates to give an overall loss for data.

Let θ_{tr} be the parameters fit from the training set \mathbf{M}_{tr} , and \mathcal{S}^* the edges in the model, three scores are computed with cross-validation:

1. the *negative entropy* of a model – i.e., the negated expected log-likelihood of the test set for the Bayesian network fitted from the training set, that is

$$\mathbf{eloss}(\mathcal{S}^*, \theta_{tr}) = -\mathbb{E}[\mathcal{L}(\mathcal{S}^*, \theta_{tr} \mid \mathbf{M}_{te})].$$

2. the *prediction error* for a single node x and its parents set X , i.e., we measure how precisely we can predict the values of x by using only the information present in its local distribution $\theta_{tr}(x)$. This parameter corresponds to computing the misclassification rates from $p_{te}(x)$, the empirical marginal probability of x estimated from the test.
3. the *posterior classification error* for a single node x and one of its parent node $y \in X$ – i.e., the values of x are predicted using only the information present in y by likelihood weighting and Bayesian posterior estimates.

⁹Consider the case where the samples are from two different unknown and heterogeneous groups, with random chance making low values to be sampled from a group that actually has a majority of high values, and vice versa. In this case, the samples will not be the best descriptor of the two groups.

See [?] for a discussion on these loss functions. The first statistics measures the *log-likelihood loss* when we “forget” some of the samples used to infer a model (indeed, the test samples); see Figure S14. Roughly, we are measuring how the model’s predictive power changes as we look at the data from different viewpoints. This is a score for a whole model, it has no scale – so cannot be used to say how good the models/data are, in any absolute sense. Nonetheless, it can be used to evaluate how “stable” a model is, for a certain dataset.

The second and third statistics measure the accuracy of the parent-set, X , for a child x ; the second statistics dealing with the whole parent set as predictor, and the third, the individual contribution of each of the parents. For these two statistics, we desire the prediction error to be low, as a measure of goodness. These are shown in Figure S13 (selected edges), S15 and S16 (all edges, prediction error).

E Supplementary Tables and Figures

Datasets (CNAs and mutations provided by TCGA)						
cancer [†]	statistics			alteration type		
	n	m	$ G $	<i>mutations</i>	<i>amplifications</i>	<i>deletions</i>
MSI-HIGH	27	16100	13798	11556	2888	1656
MSS	152	21317	16371	12417	6925	1975

[†] Samples were classified as MSI-HIGH/LOW and MSS by TCGA; see flag MSI_status in clinical data available for the COADREAD project.

Table S1: **COADREAD Data.** Data used in this study, derived from the TCGA COADREAD project [56].

MUTEX parameters		
Parameter	Value	Description
signalling-network	-	<i>MUTEX network[†]</i>
max-group-size	5	<i>maximum size of a result group</i>
first-level-random-iteration	10000	<i>number of randomisation to estimate null distribution of member p-values in groups</i>
second-level-random-iteration	100	<i>number of runs to estimate the null distribution of final scores</i>
fdr-cutoff	-	<i>false-discovery-rate cutoff maximising the expected value of true positives - false positives is estimated from data</i>
search-on-signaling-network	TRUE	<i>reduce the search space using the signalling network</i>

[†] Manually curated from Pathway Commons, SPIKE and SignalLink databases. Provided with the tool; available for download at <https://code.google.com/p/mutex/>.

MUTEX groups with score < .2			
	MSI-HIGH Groups	score	q-value
1	KRAS, BRAF,	0.095	0.48
2	NRAS, BRAF, TGFBR1	0.1677	0.45
3	ERBB2, TP53, ACVR1B, ACVR2A	0.1703	0.355
	MSS Groups	score	q-value
1	TP53, ATM,	0.051	0.34
2	ARID1A, TP53	0.075	0.193
3	KRAS, NRAS, BRAF,	0.0864	0.1975
4	CTNNB1, APC, DKK2,	0.098	0.144
5	DKK1, TP53, ATM, DKK2	0.1387	0.176
6	PIK3CA, TP53, ATM	0.164	0.207

Table S2: **MUTEX: parameters and results.** Top: Parameters used to run MUTEX on the original TCGA MSS/MSI-HIGH datasets with input CNA and somatic mutations in the pathway genes described in text. Bottom: MUTEX identified 3 and 6 groups of alterations showing a trend of mutual exclusivity in these groups with score below the suggested cutoff of 0.2.

Formulas input for testing to CAPRI[†]

	MSI-HIGH tumors	<i>description</i>
1	$(\text{NRAS:m} \oplus \text{NRAS:d}) \vee \text{KRAS:m} \vee \text{BRAF:m}$	RAF exclusivity
2	$\text{PIK3CA:m} \vee \text{ERBB2:m} \vee \text{PTEN:m} \vee \text{IGF2:d}$	MEMO group
3	$(\text{ACVR1B:m} \oplus \text{ACVR1B:d}) \vee \text{ACVR2A:m} \vee \text{TP53:m} \vee \text{ERBB2:m}$	MUTEX group
4	$(\text{NRAS:m} \oplus \text{NRAS:d}) \vee \text{TGFBR1:m} \vee \text{BRAF:m}$	MUTEX group
5	$\text{KRAS:m} \vee \text{BRAF:m}$	MUTEX group
6	$\text{ACVR1B:m} \oplus \text{ACVR1B:a}$	multiple alterations
7	$\text{NRAS:m} \oplus \text{NRAS:a}$	multiple alterations
8	$\text{FBXW7:m} \vee \text{FBXW7:a}$	multiple alterations [‡]
	MSS tumors	<i>description</i>
1	$(\text{APC:m} \oplus \text{APC:d}) \vee \text{CTNNB1:m}$	WNT exclusivity
2	$(\text{KRAS:m} \vee \text{KRAS:a}) \vee (\text{NRAS:m} \oplus \text{NRAS:a}) \vee (\text{BRAF:m} \oplus \text{BRAF:a})$	RAF exclusivity and MEMO group
3	$\text{PIK3CA:m} \vee (\text{ERBB2:m} \vee \text{ERBB2:a}) \vee (\text{PTEN:m} \oplus \text{PTEN:d}) \vee \text{IGF2:a}$	MEMO group
4	$(\text{TP53:m} \oplus \text{TP53:d}) \vee (\text{ATM:m} \oplus \text{ATM:d})$	MUTEX group
5	$(\text{TP53:m} \oplus \text{TP53:d}) \vee \text{ARID1A:m}$	MUTEX group
6	$(\text{TP53:m} \oplus \text{TP53:d}) \vee \text{ARID1A:m}$	MUTEX group
7	$(\text{APC:m} \oplus \text{APC:d}) \vee \text{CTNNB1:m} \vee \text{DKK2:m}$	MUTEX group
8	$(\text{TP53:m} \oplus \text{TP53:d}) \vee (\text{ATM:m} \oplus \text{ATM:d}) \vee \text{DKK2:m} \vee \text{DKK1:m}$	MUTEX group
9	$(\text{TP53:m} \oplus \text{TP53:d}) \vee (\text{ATM:m} \oplus \text{ATM:d}) \vee \text{PIK3CA:m}$	MUTEX group
10	$(\text{APC:m} \oplus \text{APC:d})$	multiple alterations
11	$(\text{TP53:m} \oplus \text{TP53:d})$	multiple alterations
12	$(\text{SMAD4:m} \oplus \text{SMAD4:d})$	multiple alterations
13	$(\text{TCF7L2:m} \oplus \text{TCF7L2:d})$	multiple alterations
14	$(\text{ATM:m} \oplus \text{ATM:d})$	multiple alterations
15	$(\text{NRAS:m} \oplus \text{NRAS:d})$	multiple alterations
16	$(\text{ERBB2:m} \vee \text{ERBB2:a})$	multiple alterations
17	$(\text{PTEN:m} \oplus \text{PTEN:d})$	multiple alterations
18	$(\text{SMAD2:m} \oplus \text{SMAD2:a})$	multiple alterations
19	$(\text{DKK4:m} \oplus \text{DKK4:a})$	multiple alterations
20	$(\text{SOX9:m} \oplus \text{SOX9:d})$	multiple alterations
21	$(\text{BRAF:m} \oplus \text{BRAF:a})$	multiple alterations

[†] Events type: mutation (m), deletion (d), amplification (a). Hard (\oplus) and soft (\vee) exclusivity.

[‡] Formula not included as it creates a duplicated signature in the dataset.

Table S3: **CAPRI formulas from exclusivity groups**³⁹. Formulas created for the groups, and input to CAPRI for testing. These are either derived from exclusivity groups or from genes involved in different types of alterations.

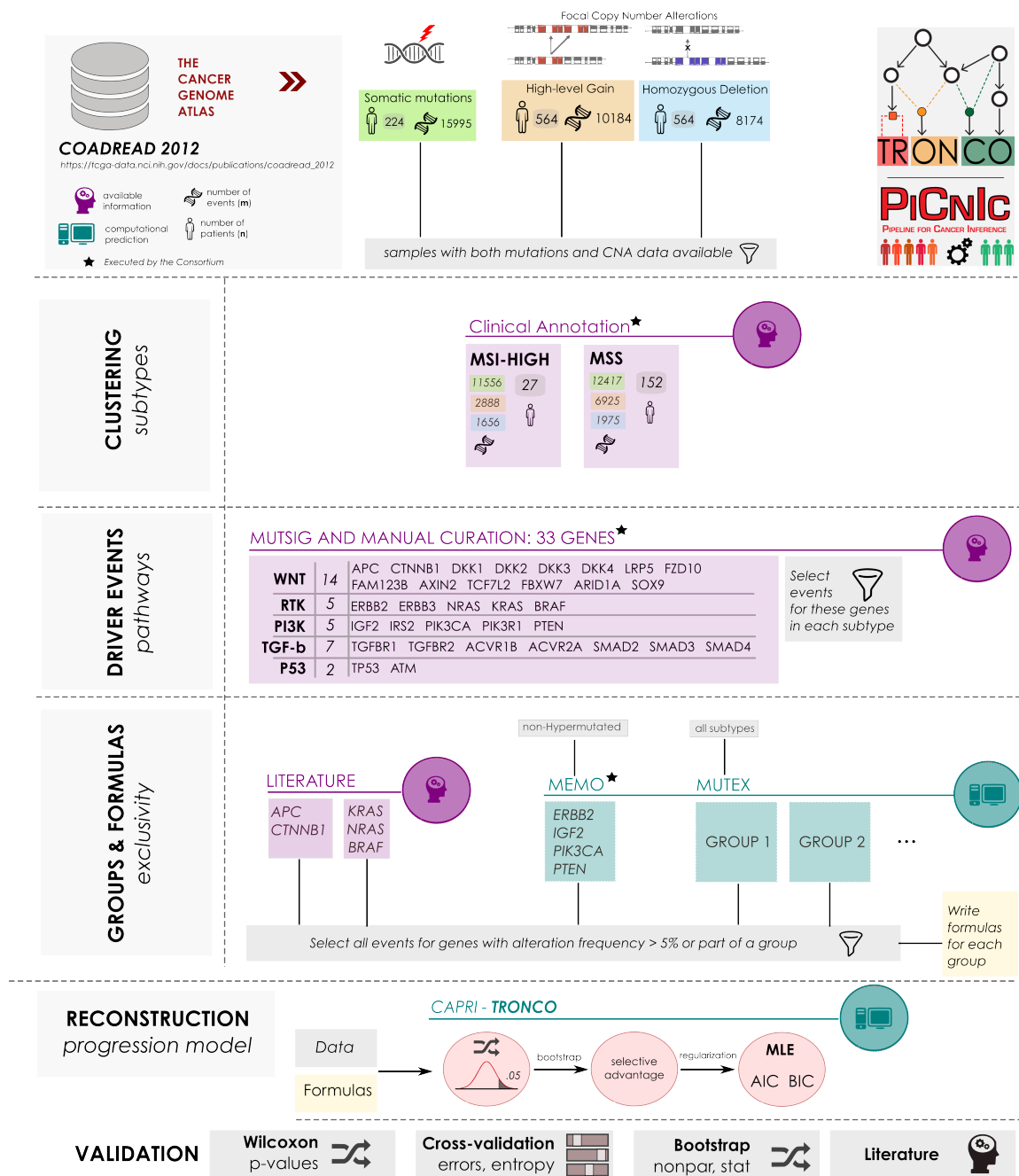


Figure S6: PicNic pipeline processing MSI-HIGH/MSS tumors. We process with PicNic Microsatellite Stable and highly unstable tumors collected from the The Cancer Genome Atlas project “Human Colon and Rectal Cancer” (subtypes annotations provided as clinical data). We implement a study on selected somatic mutations and focal CNAs in 33 driver genes manually annotated with 5 pathways in the COADREAD project. We scan groups of exclusive alterations with computational tools run by us and by TCGA, and we exploit previous knowledge on CRC; we select which alterations we input to CAPRI. Next, inference is performed with various settings of regularization and confidence. Statistical confidence of the models is assessed with standard techniques from the literature (p-values from statistical testing, bootstrap scores and cross-validation statistics).

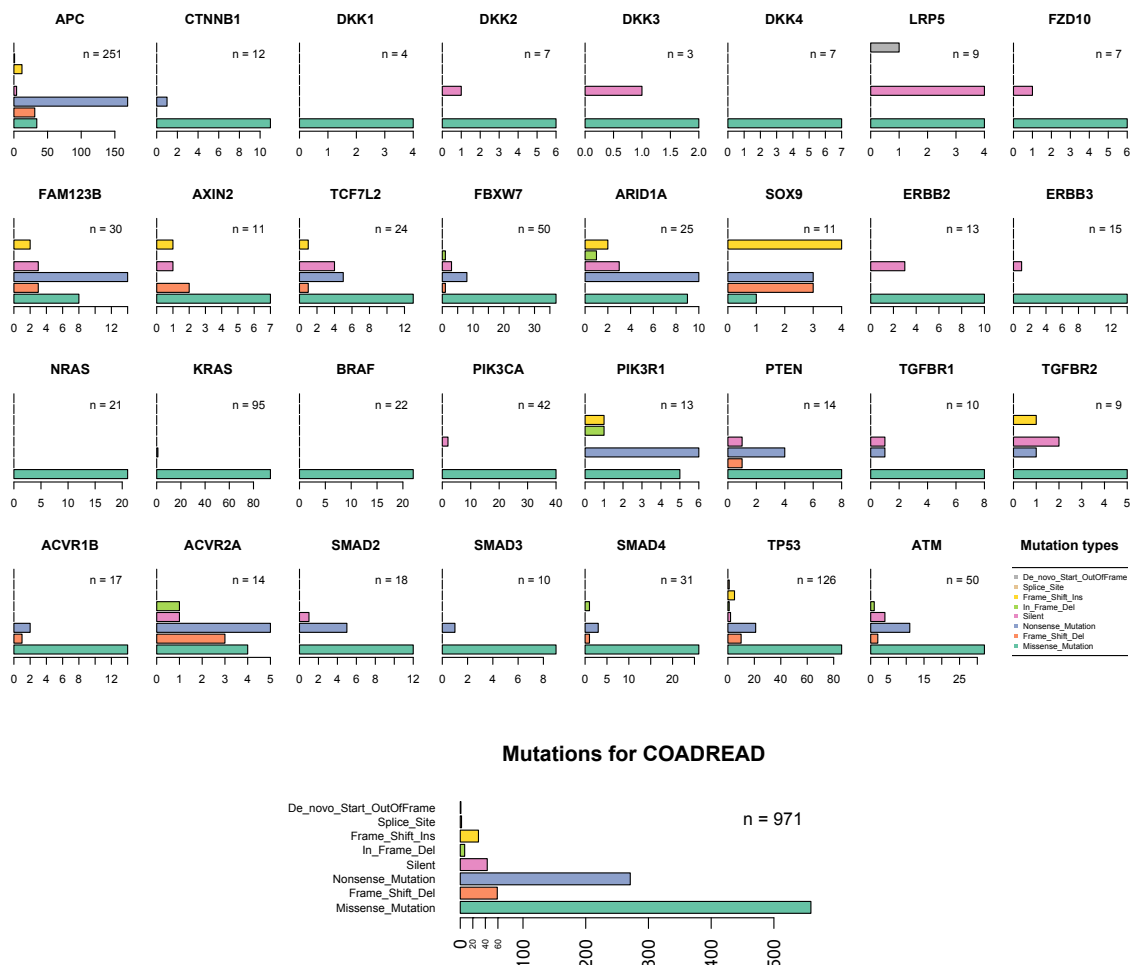


Figure S7: Mutations annotated by TCGA for the driver genes. Top: the majority of the mutations annotated by TCGA for the driver genes that we consider are *missense* – this in almost all genes and in all the cohort. Bottom: overall summation of the frequencies determine the mutations across all driver genes.

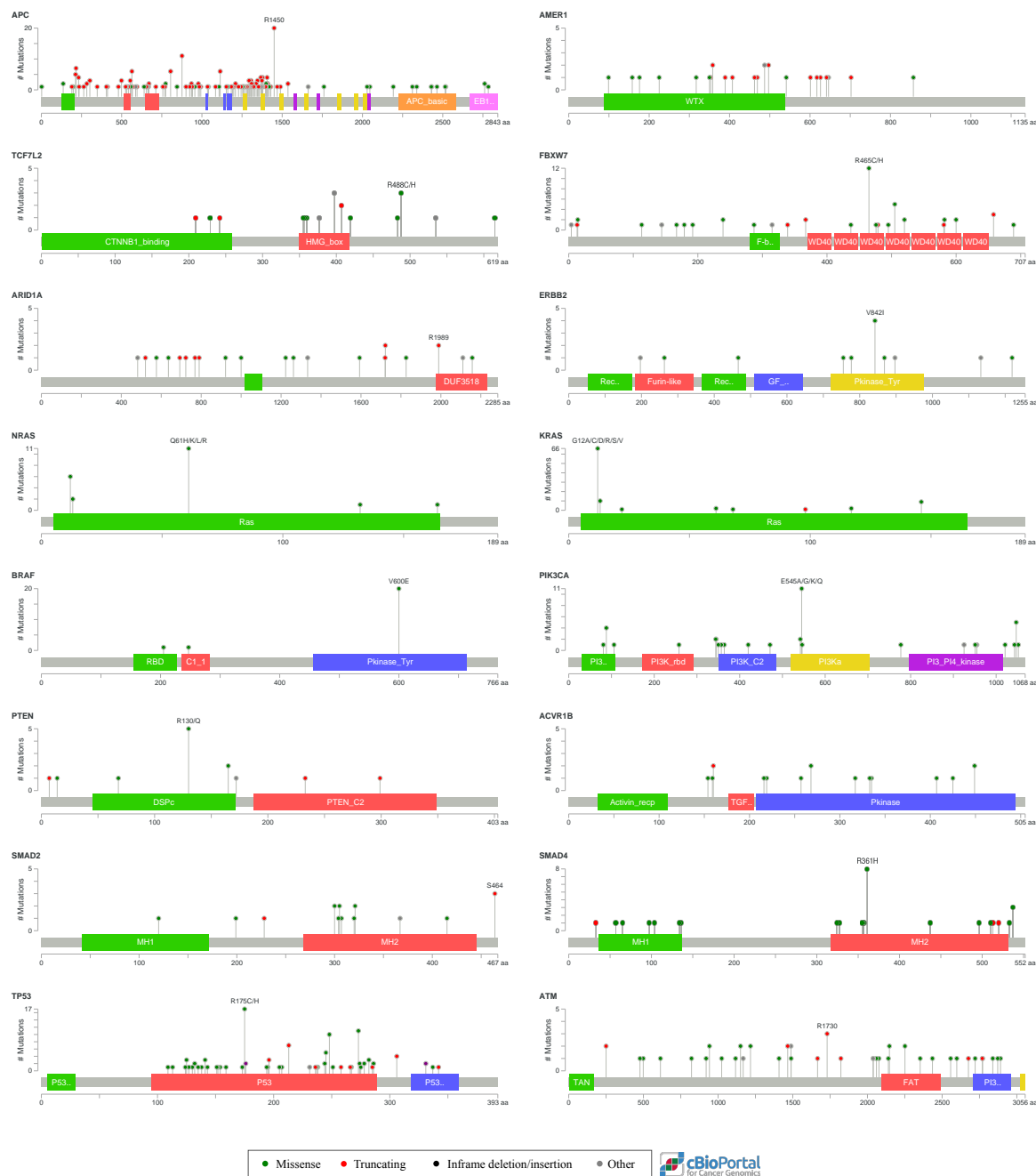


Figure S8: Lollipop diagrams of TCGA mutations. Diagrams generated from the cBio portal for the COADREAD project (see <http://www.cbioportal.org/>). These display the physical distribution of the annotated mutations for each gene. Here we shown only genes with a total mutation count greater than 15; FAM123B is called with its synonym AMER1, as in the portal.

Exclusivity groups for MSS tumors



Figure S9: **Groups of exclusive alterations for MSS tumors.** Knowledge-based groups of exclusive alterations consist of: KRAS, NRAS and BRAF genes (RAF pathway) and APC and CTNNB1 genes (WNT pathway). The MEMO [76] group identified in [56] in this cohort consists of genes PIK3CA, ERBB2, IGF2 and PTEN. Finally, 6 groups are predicted by MUTEX [77] with score below .2, one of these is equivalent to the known exclusive alterations in RAF pathway.

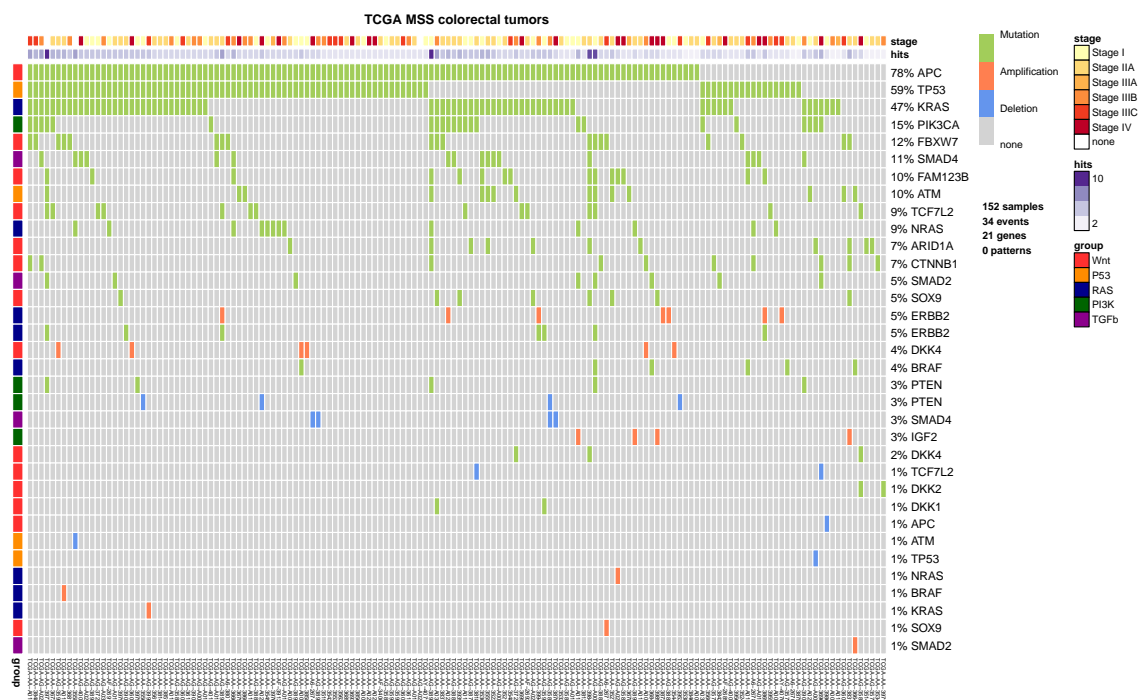


Figure S10: **Selected data for MSS tumors.** Colorectal tumors with Microsatellite Stable clinical status in the TCGA COADREAD project, restricted to 152 samples with both somatic mutations and CNA data available. 33 driver genes annotated with 5 pathways are selected from the list published in [56] to automatically detect groups of mutually exclusive alterations. Events selected for reconstruction are those involving genes altered in at least 5% of the cases, or part of group of alterations showing an exclusivity trend (see Figure S9). This dataset is used to infer the set of selective advantage relations which constitute the MSS progression model presented in the Main Text.

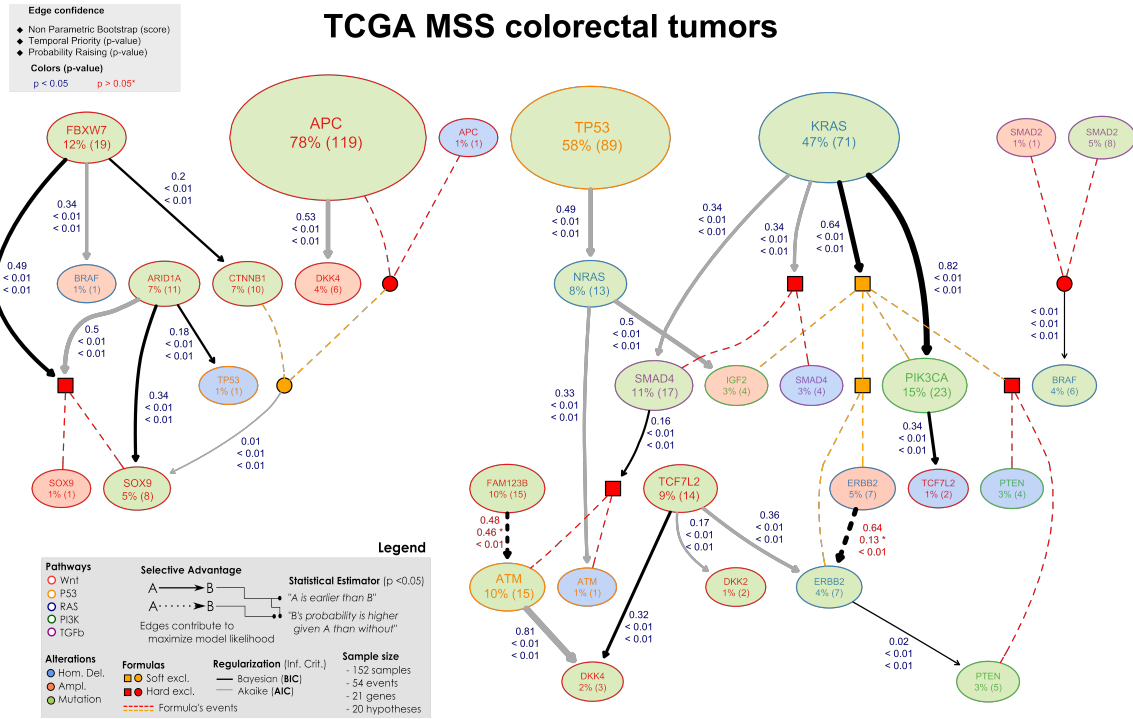


Figure S11: **Non-parametric bootstrap scores for MSS progression.** Progression model for MSS tumors with confidence shown as edge labels. The first label represents the relation confidence estimated with 100 non-parametric bootstrap iterations, the second and third are p-values for temporal priority and probability raising. Red p-values are above the minimum significance threshold of .05. See Figure 4 in the Main Text for an interpretation of this model.

TCGA MSI-HIGH colorectal tumors

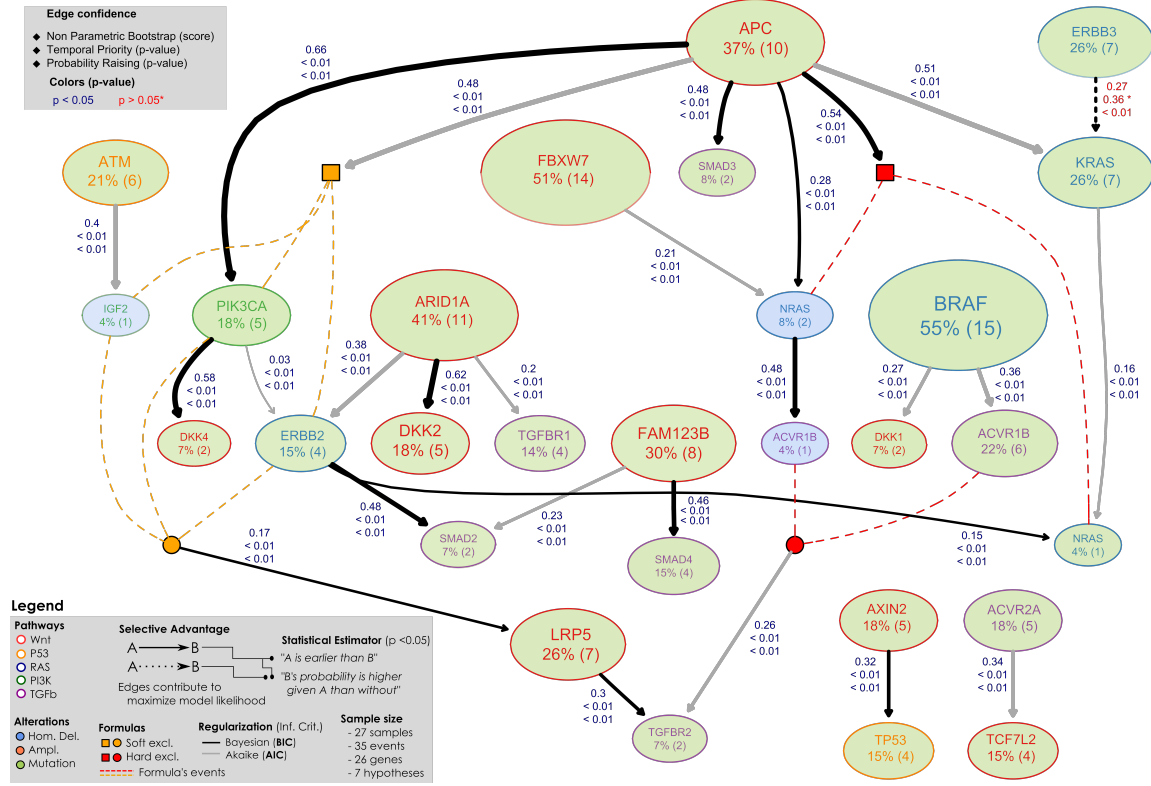


Figure S12: **Non-parametric bootstrap scores for MSI-HIGH progression.** Progression model for MSI-HIGH tumors with confidence shown as edge labels. The first label represents the relation confidence estimated with 100 non-parametric bootstrap iterations, the second and third are p-values for temporal priority and probability raising. Red p-values are above the minimum significance threshold of .05. See Figure 5 in the Main Text for an interpretation of this model.

MICRO-SATELLITE STABLE TUMORS												
BIC Relation				Bootstrap		p-values			k-fold cross-validation			
selects	#	selected	#	Non-parametric	Statistical	Selective Advantage	Data		Prediction		Posterior classification	
						Temporal Priority	Probability Raising	Hypergeometric	μ	σ	μ	σ
1 KRAS	71	PIK3CA	23	82%	100%	6,20E-92	7,63E-92	2,77E-05	1,51E-01	0,00E+00	1,51E-01	0,00E+00
2 KRAS	71	MEMO	40	64%	100%	6,64E-92	3,68E-88	7,68E-03	2,63E-01	0,00E+00	2,63E-01	0,00E+00
3 FBXW7	19	XOR_SOX9	9	49%	100%	3,15E-83	2,57E-85	1,66E-03	5,92E-02	0,00E+00	5,92E-02	0,00E+00
4 ARID1A	11	SOX9	8	34%	100%	1,73E-20	6,09E-78	9,25E-04	5,26E-02	0,00E+00	5,26E-02	0,00E+00
5 PIK3CA	23	TCF7L2	2	34%	54%	2,05E-92	5,56E-89	0,00E+00	1,32E-02	0,00E+00	1,32E-02	0,00E+00
6 TCF7L2	14	DKK4	3	32%	95%	1,15E-91	1,33E-64	6,34E-04	1,97E-02	0,00E+00	1,97E-02	0,00E+00
7 FAM123B	15	ATM	15	48%	48%	4,61E-01	2,70E-91	9,82E-04	1,01E-01	4,44E-03	1,02E-01	4,65E-03
8 ERBB2	7	ERBB2	7	64%	51%	1,27E-01	4,01E-77	5,46E-05	5,99E-02	6,54E-03	6,05E-02	6,05E-03

AIC Relation				Bootstrap		p-values			Errors			
selects	#	selected	#	Non-parametric	Statistical	Selective Advantage	Data		Prediction		Posterior classification	
						Temporal Priority	Probability Raising	Hypergeometric	μ	σ	μ	σ
1 ATM	15	DKK4	3	81%	70%	3,59E-92	2,97E-68	7,93E-04	2,70E-02	3,73E-03	1,97E-02	0,00E+00
2 APC	119	DKK4	6	53%	100%	4,70E-92	1,21E-104	0,00E+00	3,95E-02	0,00E+00	3,95E-02	0,00E+00
3 KRAS	71	SMAD4	17	50%	69%	6,06E-92	3,49E-73	3,72E-02	1,12E-01	0,00E+00	1,12E-01	0,00E+00
4 ARID1A	11	XOR_SOX9	9	50%	90%	2,20E-09	1,02E-77	1,60E-03	5,72E-02	4,44E-03	7,24E-02	0,00E+00
5 TP53	89	NRAS	13	49%	91%	5,62E-92	1,35E-69	1,22E-01	8,55E-02	0,00E+00	4,20E-01	0,00E+00

HIGHLY MICRO-SATELLITE INSTABLE TUMORS												
BIC Relation				Bootstrap		p-values			k-fold cross-validation			
selects	#	selected	#	Non-parametric	Statistical	Selective Advantage	Data		Prediction		Posterior classification	
						Temporal Priority	Probability Raising	Hypergeometric	μ	σ	μ	σ
1 APC	10	PIK3CA	5	66%	100%	2,53E-65	3,81E-72	4,73E-02	2,41E-01	4,36E-02	2,19E-01	3,24E-02
2 ARID1A	11	DKK2	5	62%	100%	3,62E-71	3,31E-76	5,72E-03	1,85E-01	0,00E+00	2,00E-01	3,12E-02
3 PIK3CA	5	DKK4	2	58%	100%	4,83E-53	2,65E-75	2,85E-02	1,37E-01	3,51E-02	1,30E-01	4,36E-02
4 APC	10	XOR_NRAS	3	54%	100%	2,51E-78	5,36E-89	0,00E+00	1,11E-01	0,00E+00	1,11E-01	0,00E+00
5 APC	10	SMAD3	2	48%	79%	9,11E-81	8,62E-81	0,00E+00	7,41E-02	0,00E+00	7,41E-02	0,00E+00
6 ERBB2	4	SMAD2	2	48%	92%	3,87E-28	6,69E-68	0,00E+00	1,41E-01	1,56E-02	1,37E-01	2,50E-02
7 NRAS	2	ACVR1B	1	48%	68%	2,93E-20	1,88E-40	0,00E+00	7,04E-02	1,17E-02	3,70E-02	0,00E+00
8 FAM123B	8	SMAD4	4	46%	100%	4,12E-51	1,98E-66	3,99E-03	1,78E-01	3,40E-02	1,96E-01	3,05E-02
9 AXIN2	5	TP53	4	32%	86%	1,32E-07	9,08E-69	1,28E-02	1,74E-01	3,05E-02	1,59E-01	3,51E-02
# LRP5	7	TGFBR2	2	30%	69%	8,32E-74	3,42E-84	0,00E+00	8,52E-02	3,51E-02	7,41E-02	0,00E+00
# ERBB3	7	KRAS	7	27%	50%	3,62E-01	4,18E-77	4,65E-03	1,56E-01	2,34E-02	1,48E-01	0,00E+00

AIC Relation				Bootstrap		p-values			Errors			
selects	#	selected	#	Non-parametric	Statistical	Selective Advantage	Data		Prediction		Posterior classification	
						Temporal Priority	Probability Raising	Hypergeometric	μ	σ	μ	σ
1 APC	10	KRAS	7	51%	100%	8,53E-34	5,84E-75	4,27E-02	1,56E-01	2,34E-02	2,59E-01	0,00E+00
2 APC	10	MEMO	8	48%	100%	3,44E-18	1,93E-64	9,10E-02	4,15E-01	4,88E-02	3,96E-01	3,92E-02

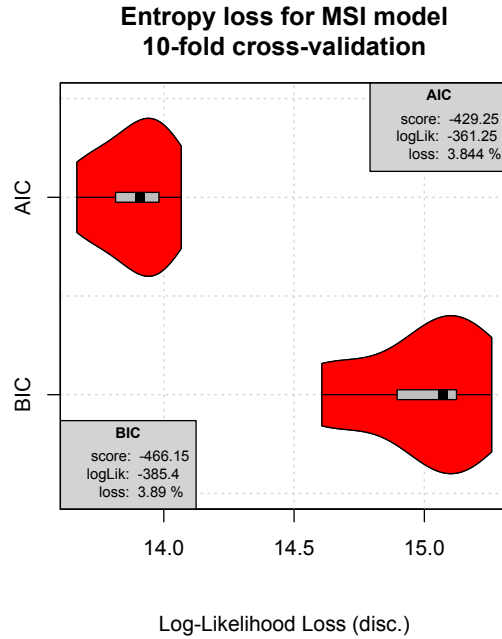
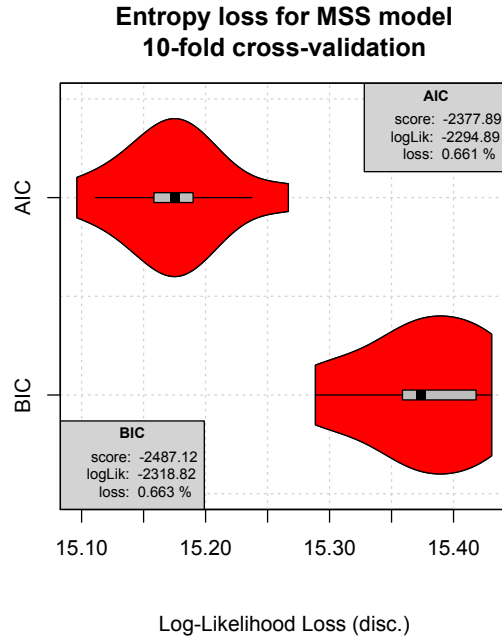
Event type	
Deletion	
Amplification	
Mutation	
Pattern	

Non-parametric minimum score	
BIC	30%
AIC	50%
approximate	

p-values	
< 0,01	
0,01 - 0,05	
> 0,05	

error	
(mean μ , stdev σ)	
< 0,1	
0,1 - 0,2	
> 0,2	

Figure S13: **COADREAD statistics for models confidence.** For BIC models we show statistics for edges with non-parametric bootstrap score approximately greater than 30%, for AIC models those greater than 50%. *i*) *p-values* (100 repetition of non-parametric bootstrap, prior to Wilcoxon testing) for each edge statistics of selective advantage (*direction and statistical dependence, and hypergeometric*). In general, the edges that we selected show very strong support ($p \ll 10^{-10}$), but for those edges connecting events with the same marginal frequencies, where we can not be confident in the edge direction ($p > 0.05$) but still we find strong statistical dependence. *(ii)* *A posteriori* model confidence against Type I and II errors estimated with *non-parametric and statistical bootstraps* (100 repetitions) – edges annotated in Figures S11 and S12. *(iii)* Values of *posterior classification and prediction errors* are estimated from 10 repetitions of 10-fold *cross-validation*. The former reports how much error is due to predicting, for each set of edges $X = \{x_1, \dots, x_n\} \rightarrow y$, the value of y according to the value of each $x_i \in X$. The latter reports the same statistics when we predict y from the whole set of parents X .

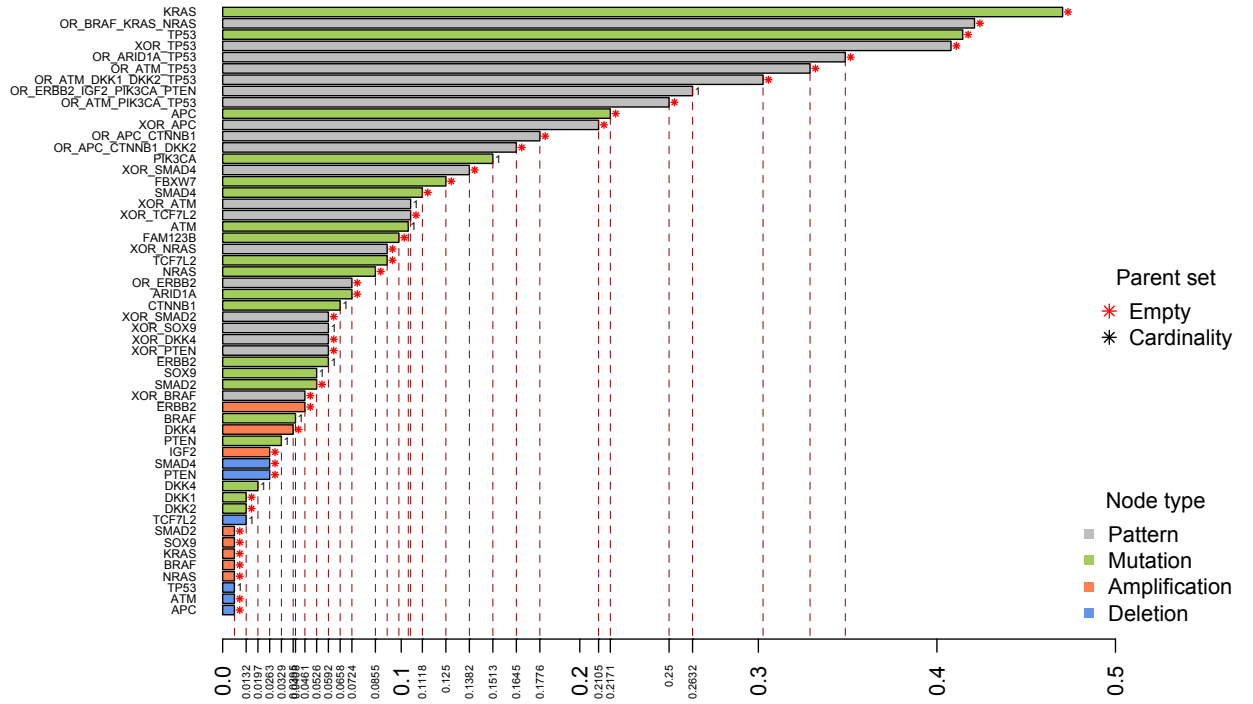


MSS						MSI-HIGH					
Model Entropy Loss											
	μ	σ	score	logLik	ratio		μ	σ	score	logLik	ratio
BIC	15,39	4,4E-02	-2487,12	-2318,82	0.664%		14,53	6,8E-01	-466,2	-385,40	3,60%
AIC	15,20	4,7E-02	-2377,89	-2294,89	0.662%		13,89	2,0E-01	-429,3	-361,25	3,80%

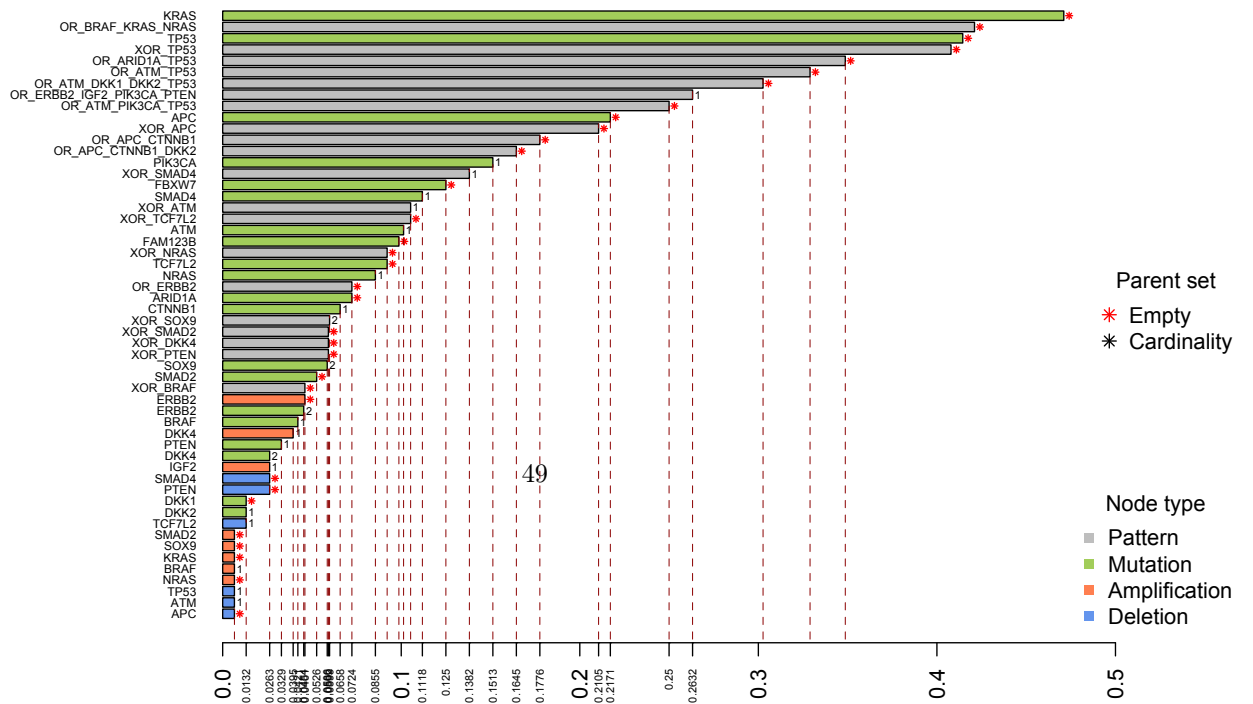
Mean (μ) and standard deviation (σ) computed with 10 independent 10-fold crossvalidation runs. The model **score**s reported; it includes both the log-likelihood contribution (**logLik**) and the regularization term for AIC/BIC. We show the average **ratio** of logLik loss with cross-validation.

Figure S14: **Entropy loss for MSI-HIGH/MSS models.** Violin plot computed from 10 runs of k -fold cross-validation with $k = 10$, where we compute the “loss of log-likelihood” at each fold. In the plot and in the table we report also the overall log-likelihood, as well as the BIC and AIC scores for the models. We present the ratio of log-likelihood loss as a measure of stability of these models for these two datasets – we can observe that the MSS models lose $< 1\%$ of their likelihood, while the MSI lose slightly more (still, $< 4\%$), possibly because of the smaller sample size. From statistical point of view, the “loss of log-likelihood” is a measure of model stability, and the “ratio of log-likelihood loss” is a measure of model stability.

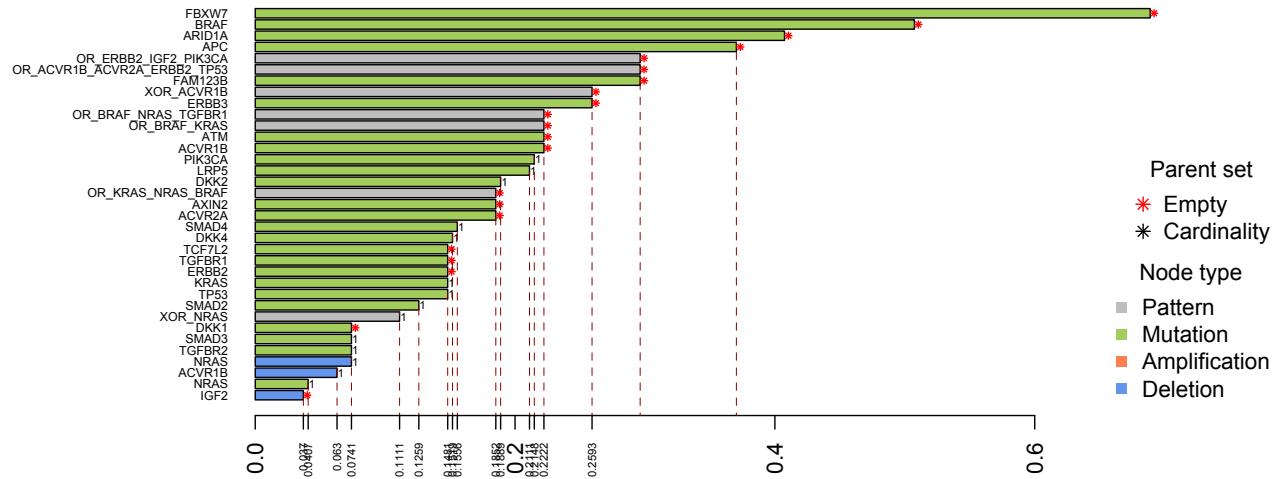
MSS Prediction Error (BIC parent set, k-fold cross-validation)



MSS Prediction Error (AIC parent set, k-fold cross-validation)



MSI Prediction Error (BIC parent set, k-fold cross-validation)



MSI Prediction Error (AIC parent set, k-fold cross-validation)

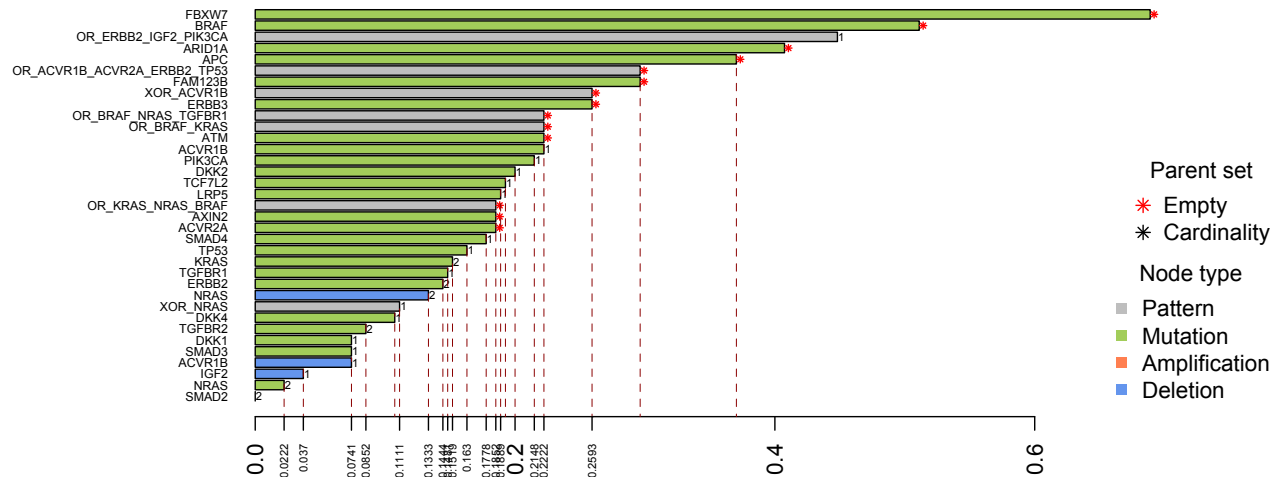


Figure S16: Prediction error for each parent set of BIC and AIC models of MSI-HIGH tumors.

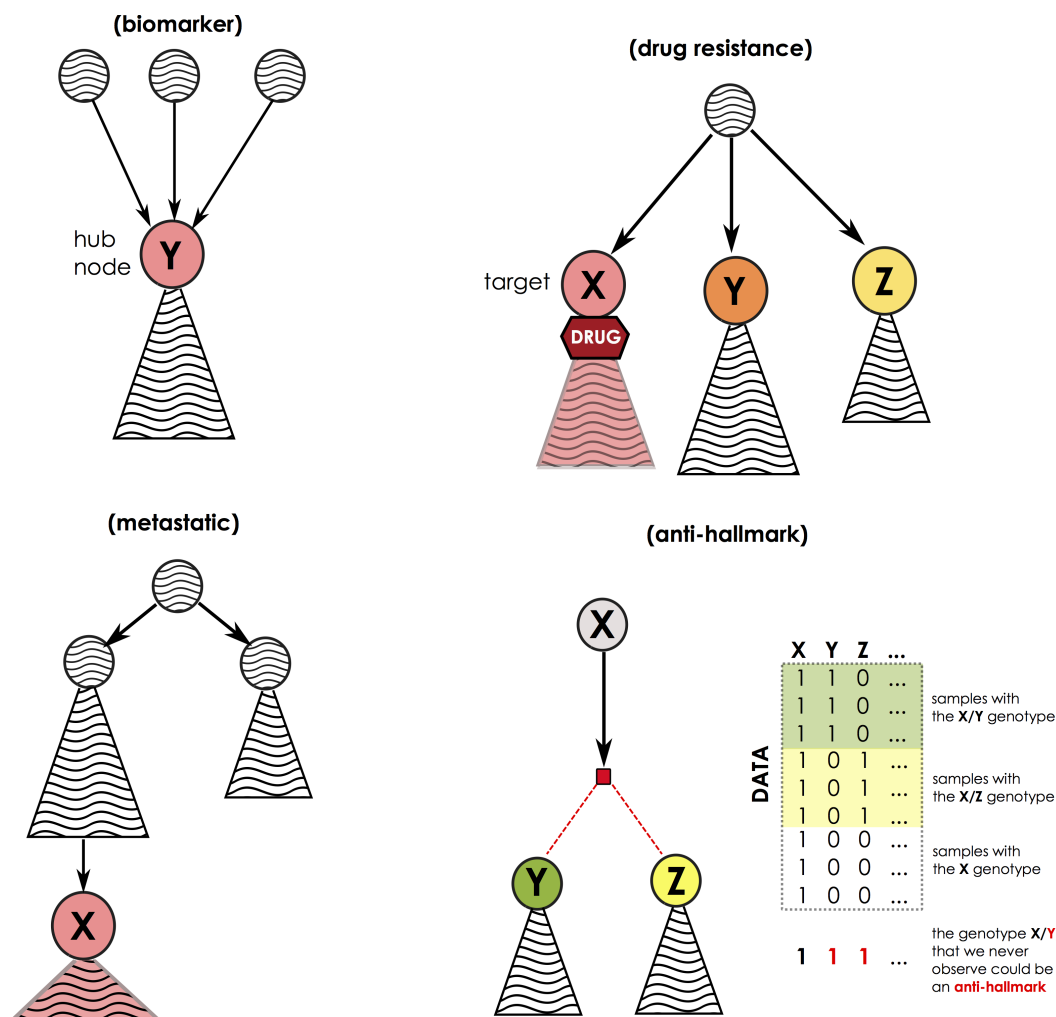


Figure S17: **Models and the phenotype that they might explain.** **(biomarker)** Independent evolutionary trajectories depicted by a model might share common routes through a certain alteration Y; that could point to a new biomarker harbored by most of the tumors under study. **(drug resistance)** When a progression model branches in many independent sub-progressions, each one identified by alterations X, Y and Z, if a certain drug is known to target only a certain type of such clones (e.g., those where biomarker X is present), we might get insights on which are the biomarkers which make the drug ineffective for certain patients (e.g., those where cancer evolves through Y and Z). **(metastatic)** When a model is extracted from data representative of various tumor stages, we might discover which “late events” are those conferring a metastatic phenotype to a tumor – X in the figures. **(anti-hallmarks)** Relation between anti-hallmarks and formulas. Exclusivity formulas allow to capture fitness-equivalent events (Y and Z in the figure), and the presence of alternative routes – here those identified by the genotypes X/Y or X/Z. These could point us to genotype/phenotype that we do not observe in our cohort – here the X/Y/Z – which could be exploited for targeted therapy if a synthetic lethality is screened among Y and Z, the anti-hallmark.